Coupling effect of $Fe^{3+}_{(aq)}$ and biological, nano-sized FeS-coated limestone on the removal of redox-sensitive contaminants (As, Sb and Cr): implications for *in situ* passive treatment of acid mine drainage

Lei Zhou[1], Faqin Dong[1], Jing Liu[1], Karen A. Hudson-Edwards[2*]

[1] *The Key Laboratory of Solid Waste Treatment and Resource Recycle, Ministry of Education, Southwest University of Science and Technology, Mianyang, 621010 China.*

[2]*Department of Earth and Planetary Sciences, Birkbeck, University of London, Malet St., London WC1E 7HX, UK.* *Corresponding author. Email: k.hudson-edwards@bbk.ac.uk

Published in: *Applied Geochemistry*

Keywords: permeable reactive barrier; biological nano-sized FeS particles; redox-sensitive contaminants; permeability; remediation

Abstract

Nano-sized FeS particles have been shown to improve the adsorption performance in permeable reactive barrier (PRB) technologies that are used to treat acid mine drainage. To investigate the coupling effect of Fe^{3+} and biological nano-sized FeS on removal of redox-sensitive contaminants and the permeability of a limestone system, Fe-reducing bacteria (FRB) and sulfate-reducing bacteria (SRB) were used to form nano-sized FeS coatings on limestone grains. For initial acidic solutions containing 0.5 mg/L As(V), Cr(VI) and Sb(V), retardation factors increase from 26, 5 and 7, respectively, in a limestone-only (pristine) system to >>367, 89 and 9, respectively, in an FeS-coated limestone system, and to 345, 367 and 308, respectively, in an FeS-$Fe^{3+}_{(aq)}$ system. The permeability coefficient of the FeS-coated limestone system is better than that of the pristine limestone system, but declines to two-thirds of the pristine limestone system in the presence of $Fe^{3+}_{(aq)}$, possibly due to the formation of secondary ferric hydroxides. XPS analysis suggests that the FeS particles are effective at reducing As(V), Sb(V) and Cr(VI) and removing them from solution. These results demonstrate that FeS particles improve retention of redox-sensitive contaminants with and without $Fe^{3+}_{(aq)}$. These new findings give new insights on the coupling effect of redox systems used in PRBs.

1. Introduction

Permeable Reactive Barrier (PRB) technologies are used to remediate acid mine drainage (AMD) by passing the AMD through a wall filled with reactive material that removes metal and metalloid elements by chemical adsorption, precipitation and/or biomineralization (Gilbert et al., 2011; Liu et al., 2014b, 2016). Limestone is the most common PRB filling material due to its low cost and ability to neutralise acidic solutions, and it has, as a result, been widely used for AMD treatment (Hedin et al., 1994; Liu et al., 2013; Lottermoser, 2010). The contaminant removal ability and permeability of the limestone filling are important factors determining the performance and service life of PRB systems. For example, the maximum adsorption capacity of limestone for As(V) is only 0.01 mg/g (Davis et al., 2007), but this can be improved significantly if the limestone is coated with reactive materials such as iron and manganese oxides (Han et al., 2011a; Liu et al., 2016). In practice, smaller limestone particles are desirable for increasing neutralization rates and adsorption performance, but these can be clogged by secondary precipitates, reducing the permeability of the system. $Fe^{3+}_{(aq)}$, derived mainly from the oxidation of pyrite (FeS_2), is the most common cation in AMD. $Fe^{3+}_{(aq)}$ can help to remove AMD contaminants by adsorption and uptake in precipitates such as ferric hydroxide ($Fe(OH)_3$) and schwertmannite ($Fe_8O_8(OH)_6SO_4$) (Boi, 2010; Soler et al., 2008; Dou et al., 2013). However, $Fe^{3+}_{(aq)}$ can negatively affect the permeability of the limestone-filled PRB due to the occlusion of pore spaces by these secondary precipitates (Boi, 2010; Soler et al., 2008). For example, Liu et al. (2013) showed that the formation of schwertmannite during treatment of AMD by zero-valent iron rapidly decreased the permeability of the PRB. To improve permeability, 'reductive walls' are often built in front of the limestone-filled PRBs to maintain a reducing environment to decrease the production of these secondary Fe(III) precipitates (Luptakova and Kusnierova, 2005; Want et al., 2014; Zagury et al., 2006). The reductive walls are filled with materials such as organic waste (Lee et al., 2010) and animal manure (Khan Eusuf Zai et al., 2010).

Nano-sized FeS particles are used as PRB filling materials, and they have been shown to have better adsorption performance than common mineral adsorbents such as zero-valent iron and other iron-bearing minerals (Zhang et al., 2010; Yanyan et al., 2012; Xiong et al., 2009; Han et al., 2011b) and to reduce contaminants such as uranium (Lee et al., 2013). In view of these properties, it is hypothesised that nano-sized FeS could improve limestone-filled PRB systems by acting as coatings on the limestone. Ferric reducing bacteria (FRB) and sulfate reducing bacteria (SRB) are ubiquitous bacteria in AMD, and they can be isolated and cultured in the laboratory (Bowell et al., 2014). They can reduce Fe^{3+} to Fe^{2+} and SO_4^{2-} to S^{2-}, and the resultant ions can then form Fe_nS_m (Sen and Johnson, 1999). These bacteria could therefore be used to form *in situ* FeS that could coat limestone particles in PRB systems. The FeS could also potentially reduce redox-sensitive contaminants in AMD, such as arsenic (As), antimony (Sb) and chromium (Cr) (Robinson, 2010), and incorporate

them via adsorption or secondary precipitation. To date, however, these hypotheses have not been tested.

In this manuscript we describe the results of an innovative study in which nano-sized FeS precipitates were formed on limestone using FRB (*Acidiphilium cryptum* JF-5) and SRB (*Desulfovibrio vlugaris miyazaki* SRB). The efficiency and mechanism of removal of elements As(V), Sb(V) and Cr(VI) from synthetic AMD, and the effects on the permeability of the system in the presence of $Fe^{3+}_{(aq)}$ were investigated. The results of the study will help to design more efficient PRB systems to remediate AMD, the most significant global issue facing the mining industry (Hudson-Edwards et al., 2011).

2. Materials and methods

2.1 Culturing of microorganisms, limestone collection and preparation of FeS-coated limestone

A. cryptum JF-5 was very kindly supplied by Friedrich Schiller of the University of Jena. To culture an acidophilic Fe(III)-reducing bacteria, an acidic Fe-tryptone soya broth (Fe-TSB) medium was prepared according to the methods described by Küsel et al. (1999). The culture medium contained 0.025% TSB-basal salts at a pH of 2.5 and was supplemented with 5 mM glucose. The medium was autoclaved at 121ºC for 15 min, cooled and dispensed under N_2. Ferric sulfate was added from an anoxic 500 mM stock solution (pH=1.7, sterilized by passing through a 0.22 μm pore size membrane) to a concentration of 35 mM Fe^{3+}. The final solution pH was approximately 2.3. In an acidic Fe-TSB medium, *A. cryptum* JF-5 bacteria can completely reduce 35 mM of Fe(Ⅲ) in about 7 days, resulting in the culture medium turning colorless (Fig S1 left).

SRB was isolated from abandoned mine tailings from the Sichuan province of China. SRB was cultured in neutral liquid medium-63 of DSMZ containing per litre: 2 g $CaCl_2 \cdot 2H_2O$, 2 g $MgSO_4 \cdot 7H_2O$, 2 g DL-Na-lactate, 1 g yeast extract, 1 g Na_2SO_4, 1g resazurin, 0.5g K_2HPO_4 and 0.5 g $FeSO_4 \cdot 7H_2O$. Both *A. cryptum* JF-5 and SRB (without ferrous sulfate in culture) were pre- incubated in an anaerobic chamber for 6 days prior to formation of the coating.

Limestone was collected from the strata of the Permian Jialingjiang Formation in Sichuan Province, China. The limestone is uniform and micritic. Limestone particles were ground and passed through a 425-850 μm (20-40 mesh) sieve. 0.5 g of prepared limestone was taken into 20 mL sample bottles and subsequently, 1 mL of *A. cryptum* JF-5 culture solution and 19 mL of SRB culture solution (without ferrous sulfate in culture) were added. The suspensions were then shaken, covered with sealing films and kept static for two days.

After two days, the supernatant was transferred into 50 mL centrifuge tubes. The coated limestone was rinsed three times using 5 mL of Milli-Q water and then dried inside the anaerobic cham-

ber. The washing waters were transferred into the same 50 mL centrifuge tubes to determine residual Fe with 0.1M HCl digestion.

2.2. Batch As(V), Sb(V) and Cr(VI) sorption experiments on FeS-coated limestone

The isothermal adsorption of As(V), Sb(V) and Cr(VI) was evaluated using batch experiments. For these, approximately 0.0124 g of Fe-S-coated limestone was added to clean sample bottles. Subsequently, 20 mL of As(V), Sb(V), Cr(VI) solutions with different concentrations (0.1, 0.5, 2.5, 10, 25, 50 mg/L) were respectively added in each sample bottle and sealed. These solutions were prepared by diluting stock solutions of ≈1 g/L As(V), Sb(V) and Cr(VI), which in turn were prepared by dissolving appropriate amounts of 4.1646 g $Na_2HAsO_4 \cdot 7H_2O$, 1.5823 g $NaSbO_3$ and 2.8287 g $K_2Cr_2O_7$ per batch, respectively (Alfa Aesar company). The sample bottles were oscillated 24 h at 150 rpm and 25℃ for to achieve equilibration sorption. The time of 24 h was based on kinetic adsorption experiments for arsenate on FeS particles, for which equilibration was achieved after 4 h. We assumed that similar times would be needed for Sb and Cr sorption, but greatly exceeded them to 24 h to ensure complete equilibration. The samples were subsequently passed through a 0.22 μm filter and analyzed for As, Sb and Cr by Inductive Coupled Plasma Emission Spectrometry (ICP-AES, iCAP6500 ThermoFisher). Each batch of adsorption experiments was done in duplicate and contained blank controls.

2.3 X-ray photoelectron spectroscopy (XPS) characterization of As(V), Sb(V) and Cr(VI)-sorbed FeS particles

To understand the effect of the FeS particles on the contaminants, XPS was used to analyse the As, Sb and Cr-sorbed nano-FeS samples prepared in the batch experiments. We did not do XPS on the column experiment materials due to the rapid oxidation of the Fe-bearing phases within them (see below) and to the difficulty in sampling the columns during the experiments. For these samples, the initial concentrations of As(V), Sb(V) and Cr(VI) were 0.5 mg/L, similar to those found in synthetic AMD solutions (Yin et al., 2008). We term these the ‘contaminant-sorbed samples’, although we acknowledge that other removal mechanisms such as surface precipitation may have occurred. These samples were prepared using the FeS formation method described in section 2.1, and by adding 2 mL of 10 mg/L As(V), Sb(V) and Cr(VI) which was diluted from 1 g/L stock solution into the initial bacterial culture mixtures to ensure the initial concentrations were 0.5 mg/L. The concentrations of As(V), Sb(V) and Cr(VI) are therefore the same as those used in the column experiments described below. These samples were collected in an anaerobic glove box and transferred using an air-tight container filled with N_2/H_2 gas to minimize exposure of the sample surfaces to atmospheric oxygen. The Al-Kα line was used as radiation source. Survey spectra were obtained with a VG-

ScientaR3000 analyzer pass energy of 70 eV. Narrow XPS scan peaks were obtained for the model compounds with a pass energy of 30 eV. Raw spectra were smoothed before being fitted using software XPSpeak software using a Shirley base line and a Gaussian-Lorentzian peak shape.

2.4. Column experiments

2.4.1 Column design and solution preparation

Column experiments were built using Perspex with a diameter of 24.70 mm and length of 146.00 mm. Two water pressure sensors were installed on the column sides 2.82 cm and 11.82 cm from the bottom inlet. The 9 cm distance between the two sensors was used to calculate the permeability coefficient. The sensors were connected to data loggers (Campbell Scientific Company, USA) and a computer, and they were calibrated with the actual water pressure, with the resultant linear relation embedded in the Loggnet software. The calibration curve is shown in Fig. S2, and overall set up of column experiment is shown in Fig. 1. The column was filled with limestone particles which had been ground and passed through a 425-850 μm (20-40 mesh) sieve to ensure good intraparticle diffusion and hydraulic conductivity for the subsequent experiments (cf., Liu et al., 2014a).

The initial acid solution (pH 2) containing 0.5 mg/L $As^{5+}_{(aq)}$, 0.5 mg/L $Sb^{5+}_{(aq)}$ and 0.5 mg/L $Cr^{6+}_{(aq)}$, which represents highly contaminated AMD (Quershi et al., 2015, Yin et al., 2008) was passed through the limestone filled column upwardly by peristaltic pump (BT100L, Leifu company China). The solution pH was adjusted using 20 v/v% H_2SO_4. This upward flow pattern can eliminate bubbles produced by the reaction between the acid solution and the limestone (Liu et al., 2013). Column experiments were also carried out in the presence of Fe^{3+} (400 mg/L), which was prepared as a stock solution by dissolving 1 g/L Fe solution ($Fe_2(SO_4)_3 \cdot 5H_2O$) and its concentration was measured by ICP-OES prior to making the synthetic AMD solution. Flow rates are also considered in this study due to their effects on contaminant removal performance and permeability. Three flow rates of 80, 110 and 150 mL/h were used in the column experiments; these were chosen based on the stability of peristaltic pump and retention ability of limestone on contaminants (Liu et al., 2014b).

2.4.2 Formation of biological nano-sized FeS particles on limestone

The columns were filled with 100 g of limestone of 425-850 μm diameter (20-40 mesh). The average pore volume was determined to be 21 mL, based on the mean of three experiments whereby the columns were completely filled with, and then drained of, water. We carried out a preliminary study to determine the best conditions for forming the maximum number of FeS particles. For this, we analysed the optimal growth of SRB and JF-5 l using optical density (OD) measurements and chemical species (e.g., SO_4^{2-} and Fe^{2+}) analysis (Fig. S3), and we also made observations of the precipi-

tates formed. The two bacteria grow most rapidly in the first 72 h of the experiment, and after this time black particles (likely FeS) were observed on the surfaces of the limestone particles.

For subsequent experiments, prepared culture solutions of SRB with an initial SO_4^{2-} concentrations of 3000 mg/L was pumped through the limestone column at a constant flow rate of 90 mL/h for 2 h using a peristaltic pump working in an up-flow mode. Immediately afterwards, the prepared JF-5 culture solution with an $Fe^{2+}_{(aq)}$ concentration of 1.96 g/L was pumped through the column at a rate of 2.5 mL/h for 12 h. The system was then allowed to rest for 6 days to allow the FeS to form; the 6-day period is based on our previous work involving SRB and JF-5 (Liu et al., 2016). The effluent samples from column experiments were collected at 1 h time intervals using a fraction collector. The pH and Eh of the effluent samples were measured using a pH meter (PB-21, Sartorius) and an Eh meter, respectively (HQ440d multi, HACH). The aqueous samples were passed through 0.45 μm filters and analyzed for Fe, Sb, As and Cr using inductively coupled plasma optical emission spectrometer (ICP-OES, 8300DV, USA).

2.4.3. Calculation of hydraulic parameters

The Convection-Dispersion Equation (CDE) is an isothermal one-dimensional continuity equation that mathematically describes the transport of contaminants in column experiments, and is especially useful for describing breakthrough conditions. The corresponding equations are:

$$\frac{\partial C}{\partial t} = \frac{D_L}{R_f}\frac{\partial^2 C}{\partial x^2} - \frac{V_X}{R_f}\frac{\partial C}{\partial x} \quad (1)$$

$$R_f = \left(1 + \frac{\rho_b}{n} K_d\right) \quad (2)$$

$$\frac{C}{C_0} = C_R = 0.5 erfc\left(\frac{Pe^{1/2}\left(1 - \frac{U}{R_f}\right)}{2\left(\frac{U}{R_f}\right)^{\frac{1}{2}}}\right) \quad (3)$$

where C is the contaminant (in this study, As, Sb or Cr) concentration (mg/L), V_x is the Darcy velocity (V_x = flow quantity/cross area of column, cm/s), t is the time during which the solute flows through the column (s), x is the coordinate in the direction of flow along the V_x direction, D_L is the longitudinal dispersion coefficient of each contaminant (cm^2/s), ρ_b is the bulk density of media (g/cm^3), n is the porosity of filled limestone column, K_d is the linear adsorption coefficient (cm^3/g),

which can be estimated using batch experiments, and R_f is the retardation factor (R_f). The retardation factor can quantitatively describe the retention ability of PRB filling materials on contaminants, and also evaluate the effect of flow rate on transport (Liu et al., 2014b). Breakthrough curves for the contaminants in this study were obtained by plotting the ratios of contaminant concentrations at outlet and inlet against pore volume.

The permeability coefficient represents the hydraulic conductivity at given hydraulic gradient. For our experiments, we calculated the hydraulic gradient using Darcy's Law:

$$Q=KiA \qquad (4)$$

where Q is the flow volume (mL/h), K is the permeability coefficient (m/d), i is the hydraulic gradient and A is the cross sectional area. In our study, Q is the flow volume of the injecting solution by peristaltic pump, i was calculated by dividing the difference of upper and bottom tensors by their distance, A is the sectional area of column, and we used these variables in Eq 4 to calculate K. Assuming that both sectional area and flow volume are constant, the permeability coefficient actually represents the permeability variation. A sensor plays the same role as a piezometer, but it can also immediately and accurately record the dynamic variation of water pressures in column.

3. Results and discussion

3.1. Batch experiments

3.1.1 Adsorption capacities of FeS-coated limestone for As(V), Sb(V) and Cr(VI) determined by batch experiments

The maximum adsorption capacities of As(V), Sb(V) and Cr(VI) on pristine limestone are 14.9, 9.9 and 9.2 μg/g, determined using the Langmuir isotherm adsorption model (Fig. 2). The removal performance is lowest for Cr(VI), in agreement with the results of Aziz et al. (2008) and Cederkvist et al. (2010). The adsorption performances of the FeS-coated limestone are significantly higher, at 35, 60 and 126 times for As, Sb and Cr, respectively, compared to the pristine limestone. The maximum adsorption capacities of the FeS-coated limestone are 517 (As), 596 (Sb) and 1160 (Cr) μg/g. This better performance is attributed to the nano-sized FeS particles coated on limestone (B in Fig. 2).

3.1.2. Removal mechanisms of As, Sb and Cr

Compared to the As XPS 3d spectra of pure $Na_2HAsO_4{\cdot}7H_2O$ (Fig. S4), which only has one peak at 44.79 eV, the As(V)-sorbed sample has many peaks occurring at energies less than 44.79 eV. This suggests that the As(V) has been reduced to lower valence species such as As(III)-O, As(0) and As(II)-S (Fig.3A). Renock et al. (2009) suggested that FeS (as mackinawite) reduces As(V) to

As(III), resulting in the formation of insoluble As_4S_4 or As(III) surface complexes depending on the order in which the phases are contacted. Dissolved sulfide can also convert As(V) to As(III), with the formation of orpiment (As_2S_3) (Gallegos et al., 2007).

The Sb XPS spectra (Fig. 3b) suggest that the biologically-formed FeS can also reduce Sb(V) to Sb(III), resulting in the formation of Sb_2S_3. The mineral stibnite (Sb_2S_3) often forms in tandem with realgar (As_4S_4) (Dickson et al., 1975). The XPS spectra for Cr (Fig. 3c) suggest that FeS is also able to convert Cr(VI) (a toxic and highly mobile form of Cr; Boursiquot et al., 2002, And et al. 1997), to a less toxic Cr(III) form. Boursiquot et al. (2002) investigated Cr(VI) reduction by inorganic synthetic mackinawite (FeS) at pH 5 and suggested that all of the chromium was reduced to a Cr(III)-bearing solid. These XPS results suggest that the FeS particles are effective at reducing As(V), Sb(V) and Cr(VI) and removing them from solution. Further work is needed to determine whether these redox-sensitive elements are incorporated into nano-sized FeS particles by co-precipitation or sorption.

3.2. Column experiments

3.2.1. Character of FeS in limestone columns

After passing the FRB and SRB through the limestone-filled columns, a dense coating of black nano-sized particles (Fig. 4), some of which have well-developed crystal faces (Fig. 4B), formed on the limestone surfaces. XRD analysis shows that the particles are mainly composed of mackinawite, but some goethite and some unknown peaks are also present (Fig. S5). Average EDX-SEM atomic proportions of five analyses of the FeS-coated limestone are 10.78% Ca, 2.585% Fe and 2.84% S.

3.2.2. Effect of FeS on transport of As(V), Sb(V) and Cr(V) in limestone in the absence of $Fe^{3+}_{(aq)}$

*C*olumn experiments more closely simulate real PRB conditions when treating AMD than batch experiments due to their incorporation of flow conditions and the ability to determine the breakthrough point of contaminant retention. The experimental contaminant breakthrough curves are modelled with the CDE using equation (1). Similar to the batch experiment results, the column experiments show that the retention ability of pristine limestone for contaminants is As (26) > Sb (7) ≈ Cr (6), similar to that determined for contaminated rivers (Sharifi et al., 2016, Sánchez España et al., 2005b). The positive retention ability for Cr contrasts with the results of other studies which claim that limestone cannot sorb Cr (Cederkvist et al., 2010; Akyol and Yolcubal, 2006). The breakthrough behaviour of Sb in pristine limestone is similar to that of Cr, but the behaviour of both are different from that of As. Arsenic and Sb are both metalloids, both lie in group 15 of the Periodic Table, have similar outer electron shell ground state valences (As: $4s_2 3d_{10} 4p_3$; Sb $5s_2 4d_{10} 5p_3$) and mostly occur as oxidised species (i.e., As(V), Sb(V), Kossoff et al., 2012) in AMD environments.

Due to their different ionic sizes (Shannon, 1976), the larger Sb(V) ion is normally octahedrally coordinated with oxygen, forming $SbO_6^{7-}{}_{(aq)}$ and As(V) is tetrahedrally coordinated with O, forming $AsO_4^{3-}{}_{(aq)}$. As a result, Sb(V) and As(V) do not normally substitute for one another in secondary AMD minerals (e.g. scorodite $FeAsO_4.2H_2O$ and tripuhyite $FeSbO_4$; Kossoff et al., 2015). The different behaviour of As(V) and Cr(VI) in this system may be due to the pH of the system: at low pH Cr(VI) forms $Cr_2O_7^{2-}{}_{(aq)}$ or $HCrO_4^{-}{}_{(aq)}$ (Motzer and Engineers, 2004), both of which exhibit different sorption behaviour to As(V). Sb and Cr completely penetrate through limestone column at ≈25 PV (1PV= 21 mL on average) (Fig. 5A). The breakthrough behavior of As fluctuates, but the removal performance of pristine limestone on As is better than that of Sb and Cr. The maximum removal capacities of limestone follow the sequence As > Sb > Cr.

The transport behaviours of As, Sb and Cr are different in the FeS-coated limestone columns (Fig. 5B). Analysis of the breakthrough curve for Sb suggests that its retardation factor increases from 7 to 9. The breakthrough point of Cr (C_e/C_0=90%) extends to more than 350 PV compared to pristine limestone of 25. The concentration of As does not exceed 0.2 during the whole whole experiment and its removal by the FeS-coated limestone is more stable than that of the pristine limestone. The breakthrough curve results suggest that the retention ability of the FeS-coated limestone is As > Cr > Sb, which is different from the sequence of the analogous batch experiments (Cr > As > Sb). This difference suggests that competitive adsorption between As and Cr may occur in the FeS-coated system, since all three ions were passed through the columns at the same time, whereas the contaminants were considered separately in the batch experiments.

3.2.3. Effect of coexisting $Fe^{3+}{}_{(aq)}$ on transport of As, Sb and Cr

The effect of $Fe^{3+}{}_{(aq)}$ on the retention ability of As, Sb and Cr in the FeS-coated limestone system was investigated to understand the behaviour of a limestone-filled PRB in a high iron environment. $Fe^{3+}{}_{(aq)}$ not only promotes oxidation of FeS, but also reduces the permeability of limestone in PRBs due to the formation of poorly crystalline ferric hydroxides (e.g., $Fe(OH)_3$; Boi, 2010; Soler et al., 2008). The breakthrough behaviours of As, Sb and Cr in pristine limestone columns in the presence of $Fe^{3+}{}_{(aq)}$ are different from those in the absence of $Fe^{3+}{}_{(aq)}$ (Fig. 6A). The retention ability is Sb > As > Cr, suggesting that in this system Fe hydroxides play an important role in retaining both As and Sb. There are obvious fluctuations in the breakthrough curve of Cr before 200 PV, which may be due to competitive adsorption between As, Sb and Cr by iron hydroxides that formed on the limestone. Sanchez España et al. (2005a) found that the scavenging of As and Cr from AMD at the Tharsis and La Zarza-Perrunal Mines, Iberian Pyrite Belt, Spain, was mainly caused by secondary iron hydroxides. These iron hydroxides retained As better than Cr: less than 0.01 mg/s As and several 100s of mg/s Cr were found in the precipitates 10 km downstream of the mines.

The retention ability of As, Sb and Cr in the FeS-coated limestone - $Fe^{3+}_{(aq)}$ column experiments (Fig. 6B) is better than those limestone and $Fe^{3+}_{(aq)}$ only (Fig. 6A). The positions of the breakthrough points of As and Sb shift by more than 100 PV to 300 PV in the FeS experiments (Fig. 6B) compared to those in the experiments without $Fe^{3+}_{(aq)}$ (Fig. 6A). The breakthrough curve for Cr is more stable in this experiment compared to that without the FeS. Fe^{3+} is a well-known oxidant of pyrite (FeS_2), and this process results in formation of ferric hydroxides (Nordstrom, 1982). It is possible that the $Fe^{3+}_{(aq)}$ in the FeS-coated limestone columns is similarly oxidising the FeS and producing ferric hydroxides that are scavenging the As, Sb and Cr. However, due to the rapid oxidation of the FeS (Fig. S6) and difficulty in sampling, we did not collect samples from this column for chemical analysis, so we were unable to confirm the presence of the ferric hydroxide. These results show that, although the FeS enhances the retention ability of limestone on As, Sb and Cr, the presence of $Fe^{3+}_{(aq)}$ also contributes to their removal. Such stable and strong retention ability simultaneously for various contaminants is desirable for long-lived PRBs.

3.2.4. Effect of flow rate on transport

Flow rate also determines the performance, hydraulic conductivity and lifetimes of PRBs. The breakthrough points of As, Sb and Cr occur at 294, 310, 253 PV, respectively, for a flow rate of 80 mL/h (Fig. 7). When the flow rate is increased to 110 mL/h, these breakthrough curves all shift to left compared to those for the flow rate of 80 mL/h; this is attributed to more rapid exhaustion of the contaminant uptake ability at the higher flow rate. The calculated retardation factors for the 110 mL/h experiments are 219 (As), 228 (Sb) and 187 (Cr), compared to 345 (As), 367 (Sb) and 308 (Cr) for the 80 mL/h experiments. The decreasing amplitude with flow rate shows that the effect of rate flow variation on Sb retention ability is largest than others. However, a further increase in the flow rate to 150 mL/h results in the As, Sb and Cr breakthrough curves shifting towards the right. The calculated retardation factors of As, Sb and Cr are 376, 492 and 192, respectively, exceeding those for the 80 mL/h flow rate by 31, 25 and 6, respectively. We interpret these increased retardation factors as being due to formation of greater quantities of secondary Fe (II or III) precipitates in the columns in the 150 mL/h experiments; these in turn increase adsorption capacity but reduce hydraulic conductivity. That Fe has accumulated in the columns is also shown by the differences between the of inlet and outlet leachate Fe concentrations (Fig. S7). A slight decline in Fe accumulation at 150-200 PV is observed in the 110 mL/h experiment (Fig. S7), and this results in improvement of the hydraulic permeability.

3.2.5. Effect of Fe^{3+}, FeS coatings and flow rates on permeability

The hydraulic conductivity of the limestone system is controlled by both physical (e.g., flow rate)

and chemical conditions (e.g., coexisting irons and species), which also determine the lifetimes of PRB. This study investigated the effect of $Fe^{3+}_{(aq)}$, FeS coatings and flow rates on the hydraulic conductivity of the experimental limestone PRB system, but we recognise that formation of other secondary minerals including gypsum ($CaSO_4 \cdot 2H_2O$) can also result in decreases in the hydraulic conductivity of PRBs (Liu et al., 2013; Boi, 2010; Booth et al., 1997).

Permeability variations in the pristine and FeS-coated limestone experiments are shown in Fig. 8A, B and C. The permeability of pristine limestone over the whole duration of the experiment is better than that of the FeS-coated limestone, and this is likely due to dissolution of the limestone by the acidic solution (Fig. 8A). However, the permeability is decreased by approximately one-third by the end of the experiment (370 PV) in the FeS-coated limestone systems. This decrease is attributed to the FeS coating which has likely occupied some of the pore volume, decreasing the cross-sectional area that the waters pass through, and to passivation and reduction of dissolution of the limestone.

The permeabilities of the pristine and the FeS-coated limestone systems change in the presence of $Fe^{3+}_{(aq)}$ (Fig. 8B). The permeability coefficient of the pristine limestone system readily decreases before 200 PV, possibly due to passivation by ferric hydroxides. The hydraulic coefficient of the FeS-coated limestone system is different to that of the pristine limestone in that it first decreases and then increases. The decrease may be due to formation of secondary ferric hydroxides, and the increase may be due to dissolution of the FeS or other Fe-bearing phases. The hydraulic conductivity of the FeS-coated limestone system is better than that in the same system without $Fe^{3+}_{(aq)}$. In addition, the FeS coating maintains a more stable hydraulic conductivity (0.6-1.0 permeability coefficient) during the whole experiment compared to that in the pristine limestone system, suggesting the former is more suitable for extending the lifetime of PRBs.

Flow rate also plays a significant effect on permeability of limestone system in the presence of $Fe^{3+}_{(aq)}$. The permeability coefficients under low flow rate (80 mL/h) and medium flow rate (110 mL/h) are both between 1.3 and 2.0. With an increase in flow rate to 150 mL/h, the permeability coefficient is initially 8.7, and gradually decreases to 2.1 by the end of the experiment (250 PV). This suggests that higher flow rates are desirable to achieve good hydraulic conductivities, although our chemical analysis shows that this system accumulates more Fe. As explained above, we suggest that this Fe accumulation is related to the reaction between the $Fe^{3+}_{(aq)}$ and the FeS, which changes the Fe speciation and results in at least partial dissolution of the solid Fe phases. This promotes the long-term development of good hydraulic conductivity during the whole experiment (Fig. 8C). A drastic increase in permeability coefficient is observed in the 110 mL/h experiment at 150 PV (C in Fig. 8), when the breakthrough of As, Sb and Cr occurs (Fig. 7). We suggest that this is related to development of preferential channels in the columns (Kapetas et al., 2014). This proposal is sup-

ported by the decrease in accumulated Fe in the 110 mL/h experiments at 150 PV (Fig. S7).

3.2.6. Coupling effect on retardation factor

Our experiments suggest that co-existing FeS and $Fe^{3+}_{(aq)}$ together affect retardation factors (Fig. 9). When pristine limestone is the filling material in the column, the retardation factors of As, Sb and Cr are 26, 7 and 6, respectively. In the presence of $Fe^{3+}_{(aq)}$, the retention ability is enhanced greatly, improving 10, 40 and 43 times respectively for As, Sb and Cr relative to pristine limestone. The permeability of limestone system decreases by 1/3 at 120 to 260 PV, however, due to the formation of iron-bearing precipitates. When the FeS coating coexists with $Fe^{3+}_{(aq)}$, the retardation factors increase further to 13, 52 and 51 times, respectively, for As, Sb and Cr with respect to pristine limestone. Thus, the FeS not only improves the retention ability of limestone system in the presence of $Fe^{3+}_{(aq)}$, but also improves the permeability of system (B, Fig. 8). This coupling effect is desirable for good PRB performance. The improvement in permeability occurs mainly in the early stages of the experiments, but we suggest that as long as quantities of FeS are sufficient, improvements in both retention ability and permeability will be pronounced.

3.2.7 Eh and pH variations of effluents

The Eh of effluents from the FeS-coated limestone systems are generally 100-150 mV lower than those of the pristine limestone system (Fig. 10), and this is likely due to the presence of FeS in the former. Maintaining such a reducing environment is desirable for PRBs with organic layers (Khan Eusuf Zai et al., 2010; Zagury et al., 2006), and this demonstrates the feasibility of our experimental system potentially being scaled up to form a PRB. The experiments with the lowest flow rate (80 mL/h) maintain a more reducing environment that those with higher flow rates. Final pH measurements (Fig. 10) suggest that the FeS coating does not affect the neutralization ability of limestone at 80 mL/h (compared C80 to P80), but when $Fe^{3+}_{(aq)}$ is present the final pH of the FeS-coated limestone (C80Fe) is lower than in the pristine limestone system (P80). Statistical analysis of pH and Eh data from C80, C110 and C150 using Mintab shows the significance level (P) is less than 0.5 (0.00 for pH and 0.012 for Eh) (Fig. S8).

4. Implications for PRB applications

Using JF-5 and SRB to form nano-sized FeS coatings on limestone-filled PRB systems not only enhances their adsorption performance for As, Sb and Cr, but also improves their hydraulic conductivities. The relative efficiency of uptake of these contaminants differs in the FeS-only and FeS-$Fe^{3+}_{(aq)}$ systems. Good hydraulic conductivity can be maintained by forming FeS coatings and increasing flow rates. Step Flushing of limestone change has been a field method avoiding the clog-

ging of system (Santomartino and Webb, 2007; Caraballo et al., 2009). The $Fe^{3+}_{(aq)}$ and FeS coating together affect iron speciation and transport, which in turn affect hydraulic conductivity. High concentrations of $Fe^{3+}_{(aq)}$ can reduce the positive effect of the FeS coating on hydraulic conductivity. Improving the load of FeS or building a separate FeS-filled wall prior to the limestone wall in a PRB system may overcome these difficulties.

5. Conclusions

This was the first attempt to investigate the effect of biologically formed nano-sized FeS on the retention of aqueous As(V), Sb(V) and Cr(VI) in limestone-filled simulated PRB systems, and on hydraulic conductivity. Our major findings are that:

(1) For As, Cr and Sb, the retardation factors increase in the FeS-coated limestone system to >>367, 89 and 9, respectively, compared to pristine limestone (26, 5, 7), and increase further in the FeS-$Fe^{3+}_{(aq)}$ system to 345, 367 and 308.

(2) The permeability coefficient of the FeS-coated limestone system is better than that of the pristine limestone system, but declines to two-thirds of the pristine limestone system in the presence of $Fe^{3+}_{(aq)}$, possibly due to the formation of secondary ferric hydroxides

(3) XPS analysis suggests that the FeS particles are effective at reducing As(V), Sb(V) and Cr(VI) and removing them from solution.Further work is needed to elucidate the mechanisms of uptake by the FeS and the secondary ferric hydroxides that are likely forming in the columns.

Acknowledgments

This study was supported by the National Basic Research Program of China (973 Program: 2014CB846003).

References

Akyol, N.H., Yolcubal, I., 2006. Retention and transport of hexavalent chromium in calcareous karst soils. Turk. J. Earth Sci. 16, 363-379.

And, R.R.P., Fendorf, S., Fendorf, M., 1997 Reduction of hexavalent chromium by amorphous iron sulfide. Environ. Sci. Technol. 31(7), 2039-2044.

Aziz, H.A., Adlan, M.N., Ariffin, K.S., 2008. Heavy metal (Cd, Pb, Zn, Ni, Cu and Cr(III)) removal from water in Malaysia: Post treatment by high quality limestone. Bioresource Technol. 99(6), 1578-1583.

Bigham, J.M., Nordstrom, D.K., 2000. Iron and aluminum hydroxysulfates from acid sulfate waters. Rev. Mineral. Geochem. 40, 351-403.

Boi, M., 2010. The passivation of calcite by acid mine water. Column experiments with Fe(III)-

SO_4-H^+ and Fe(III)-Cl-H^+ solutions at pH 2. Appl. Geochem. 23, 3579-3588.

Booth, J., Hong, Q., Compton, R.G., Prout, K., Payne, R.M., 1997. Gypsum overgrowths passivate calcite to acid attack. J. Colloid Interf. Sci. 192(1), 207-214.

Boursiquot, S., Mullet, M., Ehrhardt, J.J., 2002. XPS study of the reaction of chromium (VI) with mackinawite (FeS). Surf. Interf. Anal. 34(1), 293–297.

Bowell, R.J., Alpers, C.N., Jamieson, H.E., Nordstrom, D.K., Majzlan, J., Eds., 2014. Arsenic: Environmental Geochemistry, Mineralogy, and Microbiology. Rev. Mineral. Geochem. 79.

Caraballo, M.A., Rötting, T.S., Macías, F., Nieto, J.M., Ayora, C., 2009. Field multi-step limestone and MgO passive system to treat acid mine drainage with high metal concentrations. Appl. Geochem. 24(12), 2301-2311.

Cederkvist, K., Holm, P.E., Jensen, M.B., 2010. Full-scale removal of arsenate and chromate from water using a limestone and ochreous sludge mixture as a low-cost sorbent material. Water Environ. Res. 82(5), 401-408.

Davis, A., Webb, C., Dixon, D., Sorensen, J., Dawadi, S., 2007. Arsenic removal from drinking water by limestone-based material. Min. Eng. 59(2), 71.

Dickson, F. W., Radtke, A. S., Weissberg, B. G., Heropoulos, C., 1975. Solid solutions of antimony, arsenic, and gold in stibnite (Sb_2S_3), orpiment (As_2S_3), and realgar (As_2S_2). Econ. Geol. 70(3), 591-594.

Dou, X., Mohan, D., Pittman, C.U., 2013. Arsenate adsorption on three types of granular schwertmannite. Water Res. 47(9), 2938-2948.

Gallegos, T.J., Hyun, S.P., Hayes, K.F., 2007. Spectroscopic investigation of the uptake of arsenite from solution by synthetic mackinawite. Environ. Sci. Technol. 41(41), 7781-7786.

Gibert, O., Rötting, T., Cortina, J. L., Pablo, J. D., Ayora, C., & Carrera, J., Bolzicco, J., 2011. In-situ remediation of acid mine drainage using a permeable reactive barrier in Aznalcóllar (SW Spain). J. Hazard. Mater. 191(191), 287-95.

Han, Y.-S., Gallegos, T.J., Demond, A.H., Hayes, K.F., 2011a. FeS-coated sand for removal of arsenic (III) under anaerobic conditions in permeable reactive barriers. Water Res. 45(2), 593-604.

Han, Y.S., Jeong, H.Y., Demond, A.H., Hayes, K.F., 2011b. X-ray absorption and photoelectron spectroscopic study of the association of As(III) with nanoparticulate FeS and FeS-coated sand. Water Res. 45(17), 5727-5735.

Hedin, R.S., Watzlaf, G.R., Nairn, R.W., 1994. Passive treatment of acid mine drainage with limestone. J. Environ. Qual. 23(6), 1338-1345.

Hudson-Edwards, K.A., Jamieson, H.E., Lottermoser, B.G., 2011. Mine wastes: past, present, future. Elements 7, 375-380.

Kapetas, L., Dror, I., Berkowitz, B., 2014. Evidence of preferential path formation and path

memory effect during successive infiltration and drainage cycles in uniform sand columns. J. Contam. Hydrol. 165(9), 1-10.

Khan Eusuf Zai, A., Horiuchi, T., Matsui, T., Meherunnesa, D., 2010. Residual effects of compost and green manure of pea with other organic wastes on nutrient-use efficiency of successive rice after wheat. Comm. Soil Sci. Plant Anal. 41(18), 2154-2169.

Kossoff, D., Hudson-Edwards, K.A., Dubbin, W.E., Alfredsson, M., Geraki, T., 2012. Cycling of As, P, Pb and Sb during weathering of mine tailings: implications for fluvial environments. Miner. Mag. 76, 1209-1228.

Kossoff, D., Welch, M.D., Hudson-Edwards, K.A., 2015. Scorodite precipitation in the presence of antimony. Chem. Geol. 406, 1-9.

Küsel, K., Dorsch, T., Acker, G., Stackebrandt, E., 1999. Microbial reduction of Fe (III) in acidic sediments: isolation of Acidiphilium cryptum JF-5 capable of coupling the reduction of Fe (III) to the oxidation of glucose. Appl. Environ. Microbiol. 65(8), 3633-3640.

Lee, S., Kim, S., Jeon, B., Bhatnagar, A., Ji, S., Youngwook, C., Lee, G., 2010. Activity of sulfate reducing bacteria in successive alkalinity producing system: Part I-effect of temperature. Research J. Chem. Environ. 14(4), 67-73.

Lee, S.Y., Baik, M.H., Cho, H.-R., Jung, E.C., Jeong, J.T., Choi, J.W., Lee, Y.B., Lee, Y.J., 2013. Abiotic reduction of uranium by mackinawite (FeS) biogenerated under sulfate-reducing condition. J. Radioanal. Nucl. Chem. 296(3), 1311-1319.

Liu, J., Cheng, H., Zhao, F., Dong, F., Frost, R.L., 2013. Effect of reactive bed mineralogy on arsenic retention and permeability of synthetic arsenic-containing acid mine drainage. J. Colloid Interf. Sci. 394, 530-538.

Liu, J., Huang, X., Liu, J., Wang, W.Q., Zhang, W., Dong, F.Q., 2014a. Adsorption of arsenic(V) on bone char: batch, column and modeling studies. Environ. Earth Sci. 72(6), 2081-2090.

Liu, J., Huang, X., Liu, J., Wang, W., Zhang, W., Dong, F., 2014b. Experimental and model studies on comparison of As (III and V) removal from synthetic acid mine drainage by bone char. Miner. Mag. 78(1), 73-89.

Liu, J., He, L., Dong, F., Hudson-Edwards, K.A., 2016. The role of nano-sized manganese coatings on bone char in removing arsenic(V) from solution: Implications for permeable reactive barrier technologies. Chemosphere 153, 146-154.

Lottermoser, B.G., 2010. Mine Wastes. Springer, Berlin Heidelberg.

Luptakova, A., Kusnierova, M., 2005. Bioremediation of acid mine drainage contaminated by SRB. Hydrometallurgy 77(1), 97-102.

Motzer, W.D., Engineers, T., 2004. Chemistry, geochemistry, and geology of chromium and chromium compounds. In: Chromium(VI) Handbook. J. Guertin, C.P. Avakian and J.A. Jacobs, (eds).

CRC Press, pp. 23-91.

Nordstrom, D.K., 1982. Aqueous pyrite oxidation and the consequent formation of secondary iron minerals. In: Kittrick, J.F., Fanning, D.S. & Hossner, L.R. (eds.) Acid Sulfate Weathering. Soil Science Society of America Special Publication, 10, 37-56.

Qureshi, A., Maurice, C., Öhlander, B., 2015. Potential of coal mine waste rock for generating acid mine drainage. J. Geochem. Explor. 160, 44-54.

Renock, D., Gallegos, T., Utsunomiya, S., Hayes, K., Ewing, R.C., Becker, U., 2009. Chemical and structural characterization of As immobilization by nanoparticles of mackinawite (FeSm). Chem. Geol. 268, 116-125.

Robinson, B.C., 2010. Mine Drainage and Related Problems. Nova Science Publishers, Hauppauge NY.

Sánchez-España, J., López Pamo, E., Pastor, E.S., Andrés, J.R., Rubí, J.A.M., 2005a. The natural attenuation of two acidic effluents in Tharsis and La Zarza-Perrunal mines (Iberian Pyrite Belt, Huelva, Spain). Environ. Geol. 49, 253-266.

Sánchez España, J., López Pamo, E., Santofimia, E., Aduvire, O., Reyes, J., Barettino, D., 2005b. Acid mine drainage in the Iberian Pyrite Belt (Odiel river watershed, Huelva, SW Spain): geochemistry, mineralogy and environmental implications. Appl. Geochem. 20(7), 1320-1356.

Santomartino, S., Webb, J.A., 2007. Estimating the longevity of limestone drains in treating acid mine drainage containing high concentrations of iron. Appl. Geochem. 22(11), 2344-2361.

Sen, A.M., Johnson, B., 1999. Acidophilic sulphate-reducing bacteria: candidates for bioremediation of acid mine drainage. Process Met. 9, 709-718.

Shannon, R.D., 1976. Revised effective ionic radii and systematic studies of interatomic distances in halides and chalcogenides. Acta Crystallogr. A32, 751-767.

Sharifi, R., Moore, F., Keshavarzi, B., 2016. Mobility and chemical fate of arsenic and antimony in water and sediments of Sarouq River catchment, Takab geothermal field, northwest Iran. J. Environ. Manage.170, 136-144.

Soler, J.M., Boi, M., Mogollón, J.L., Cama, J., Ayora, C., Nico, P.S., Tamura, N., Kunz, M., 2008. The passivation of calcite by acid mine water. Column experiments with ferric sulfate and ferric chloride solutions at pH 2. Appl. Geochem. 23, 3579-3588.

Wang, J., Sickinger, M., Ciobota, V., Herrmann, M., Rasch, H., Rösch, P., Popp, J., Küsel, K., 2014. Revealing the microbial community structure of clogging materials in dewatering wells differing in physico-chemical parameters in an open-cast mining area. Water Res. 63, 222-233.

Xiong, Z., He, F., Zhao, D., Barnett, M.O., 2009. Immobilization of mercury in sediment using stabilized iron sulfide nanoparticles. Water Res. 43(20), 5171-5179.

Yanyan, G., Yuanyuan, L., Zhong, X., Dawn, K., Dongye, Z., 2012. Immobilization of mercury in

field soil and sediment using carboxymethyl cellulose stabilized iron sulfide nanoparticles. Nanotechnol. 23(29), 294007.

Yin, H., Cao, L., Xie, M., Chen, Q., Qiu, G., Zhou, J., Wu, L., Wang, D., Liu, X., 2008. Bacterial diversity based on 16s rrna and gyrb genes at Yinshan mine, China. Syst. Appl. Microbiol. 31(4), 302–311.

Zagury, G.J., Kulnieks, V.I., Neculita, C.M., 2006. Characterization and reactivity assessment of organic substrates for sulphate-reducing bacteria in acid mine drainage treatment. Chemosphere 64(6), 944-954.

Zhang, M., Wang, Y., Zhao, D., Pan, G., 2010. Immobilization of arsenic in soils by stabilized nanoscale zero-valent iron, iron sulfide (FeS), and magnetite (Fe_3O_4) particles. Chinese Sci. Bull. 55(4), 365-372.

FIGURE CAPTIONS

Figure 1. Design of the biological nano-sized FeS-coated limestone column.

Figure 2. Isothermal adsorption As(V), Sb(V) and Cr(VI) on pristine limestone (A) and FeS-coated limestone (B). Error bars represent the standard deviation of each experiment.

Figure 3. XPS As 3d, Sb 3d and Cr 2p peak spectra for As(V), Sb(V) and Cr(VI) reacted with biologically-formed FeS.

Figure 4. SEM images (A and B) and TEM images (C and D) of FeS particles.

Figure 5. Breakthrough curves of As, Sb and Cr in pristine (A) and FeS-coated limestone (B) columns at a flow rate of 80 mL/h (pH=2, initial As, Sb and Cr concentrations 0.5 mg/L, C: FeS-coated limestone, P: pristine limestone).

Figure 6. Breakthrough curves of As, Sb and Cr in pristine limestone in the presence of $Fe^{3+}_{(aq)}$ (A) and of FeS-coated limestone in the presence of $Fe^{3+}_{(aq)}$ (B) (pH=2, initial As, Sb and Cr concentrations 0.5 mg/L, C: FeS-coated limestone, P: pristine limestone Fe: 400 mg/L Fe).

Figure 7. Breakthrough curves of As, Sb and Cr in FeS-coated limestone columns in the presence of $Fe^{3+}_{(aq)}$ and with different flow rates (black: 80 mL/h; red: 110 mL/h; blue: 150 mL/h).

Figure 8. Permeabilities of pristine and FeS-coated limestone systems (C: FeS-coated limestone, P: pristine limestone).

Figure 9. Schematic diagram illustrating the effects of FeS-coated limestone and $Fe^{3+}_{(aq)}$ on retention factors at a flow rate of 80 mL/h.

Figure 10. Eh and pH values of effluents of the pristine and FeS-coated limestone systems.

Figure 1.

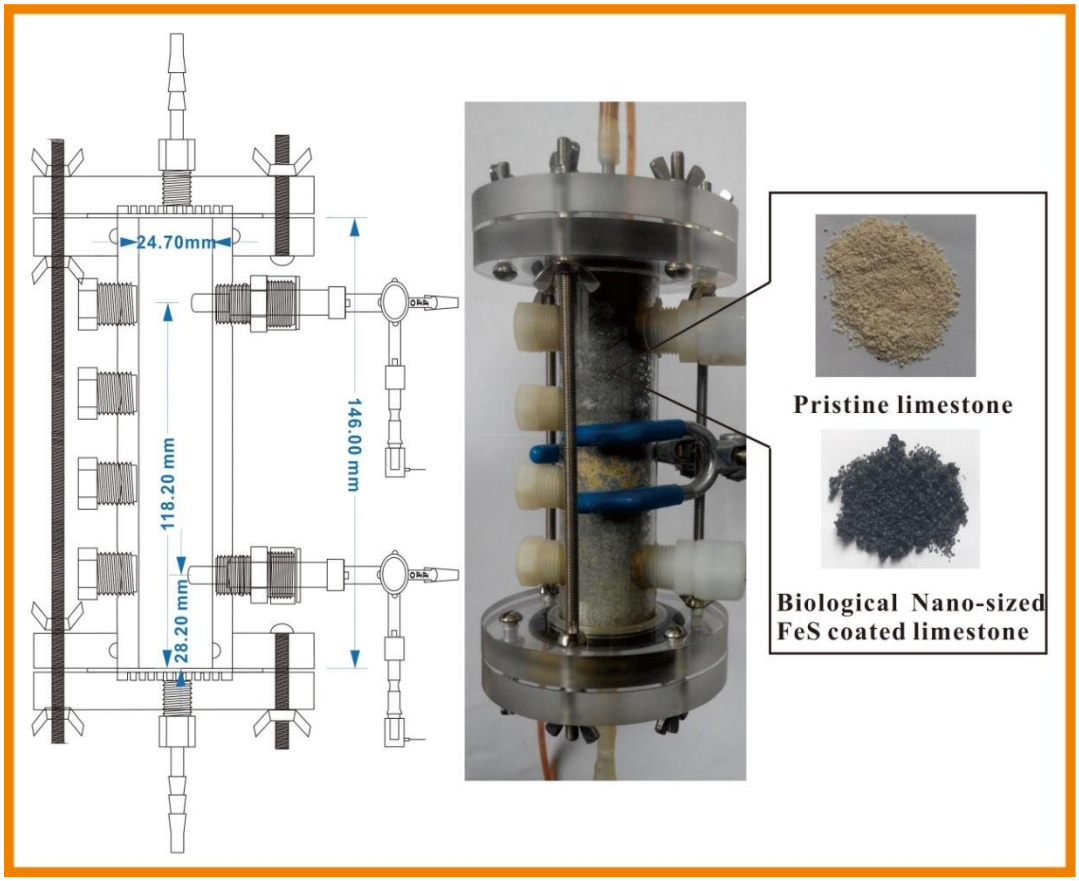
24.70mm
118.20 mm
28.20 mm
146.00 mm
Pristine limestone
Biological Nano-sized
FeS coated limestone

Figure 2.

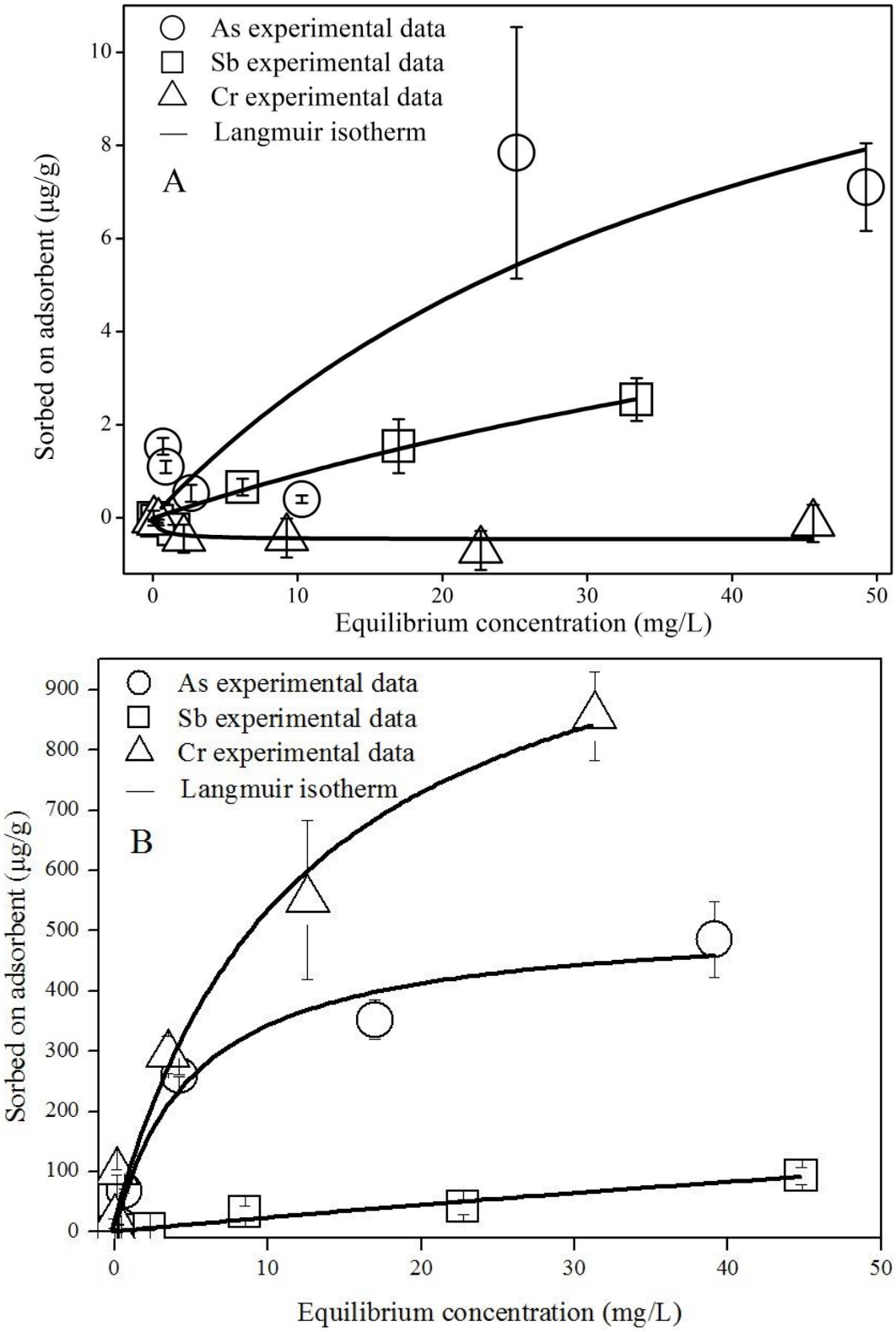
As experimental data
Sb experimental data
Cr experimental data
Langmuir isotherm
A
Sorbed on adsorbent (µg/g)
Equilibrium concentration (mg/L)
B

Figure 3.

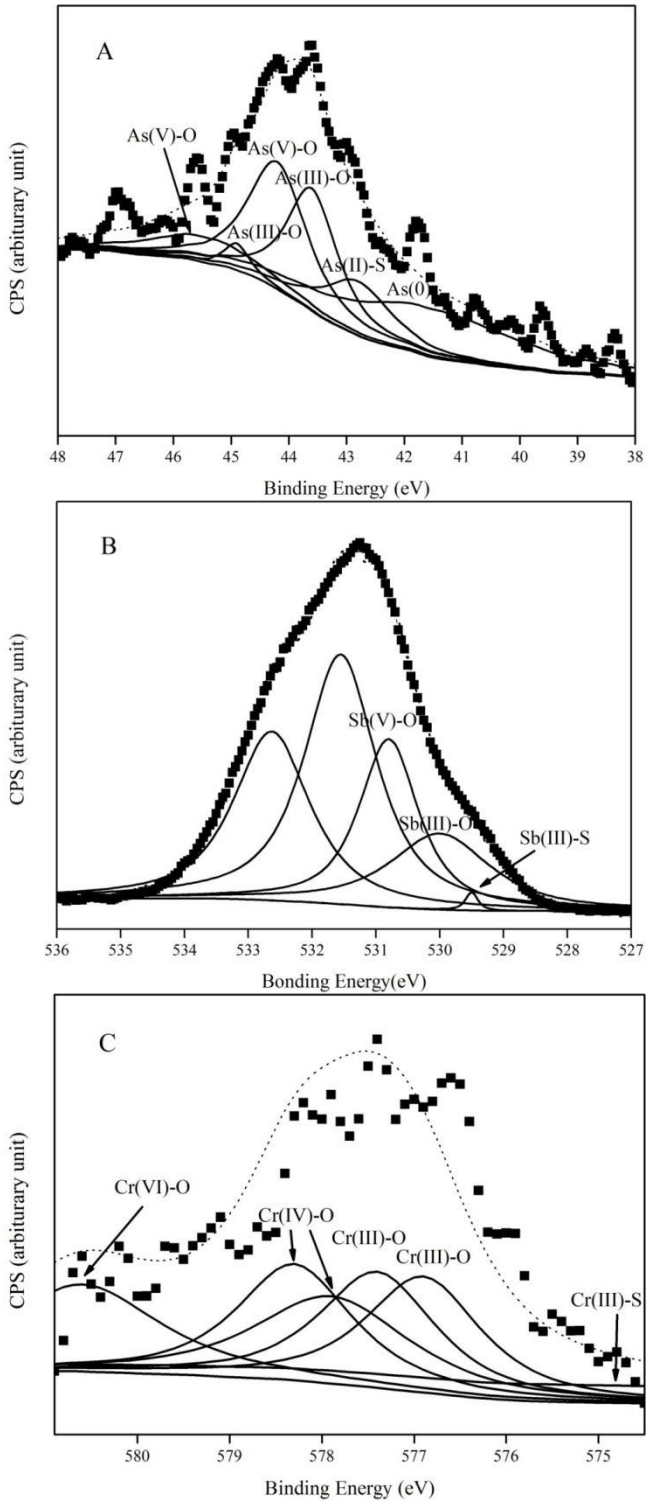
A
As(V)-O
As(V)-O
As(III)-O
As(III)-O
As(II)-S
As(0)
CPS (arbituraru unit)
48 47 46 45 44 43 42 41 40 39 38
Binding Energy (eV)
B
Sb(V)-O
Sb(III)-O
Sb(III)-S
CPS (arbituraru unit)
536 535 534 533 532 531 530 529 528 527
Bonding Energy(eV)
C
Cr(VI)-O
Cr(IV)-O
Cr(III)-O
Cr(III)-O
Cr(III)-S
CPS (arbituraru unit)
580 579 578 577 576 575
Binding Energy (eV)

Figure 4.

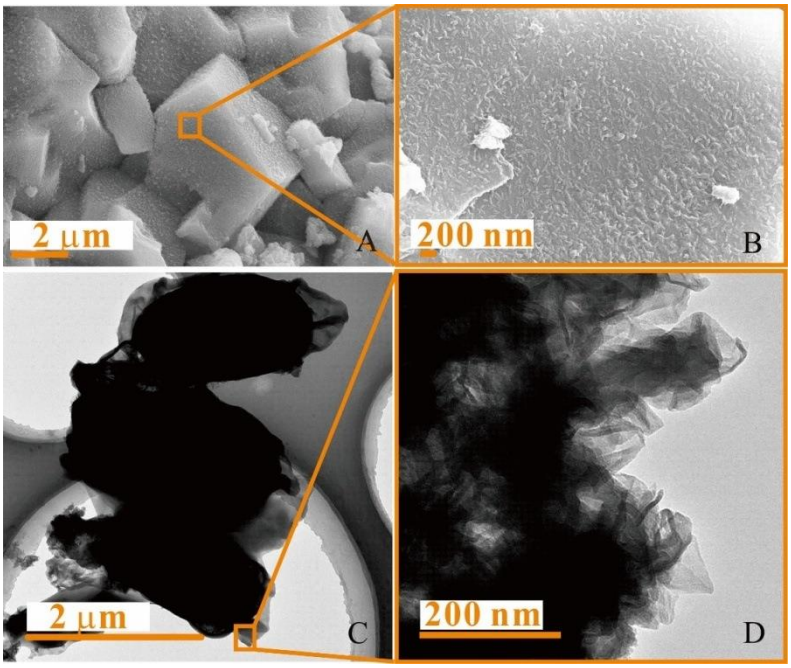

Figure 5.

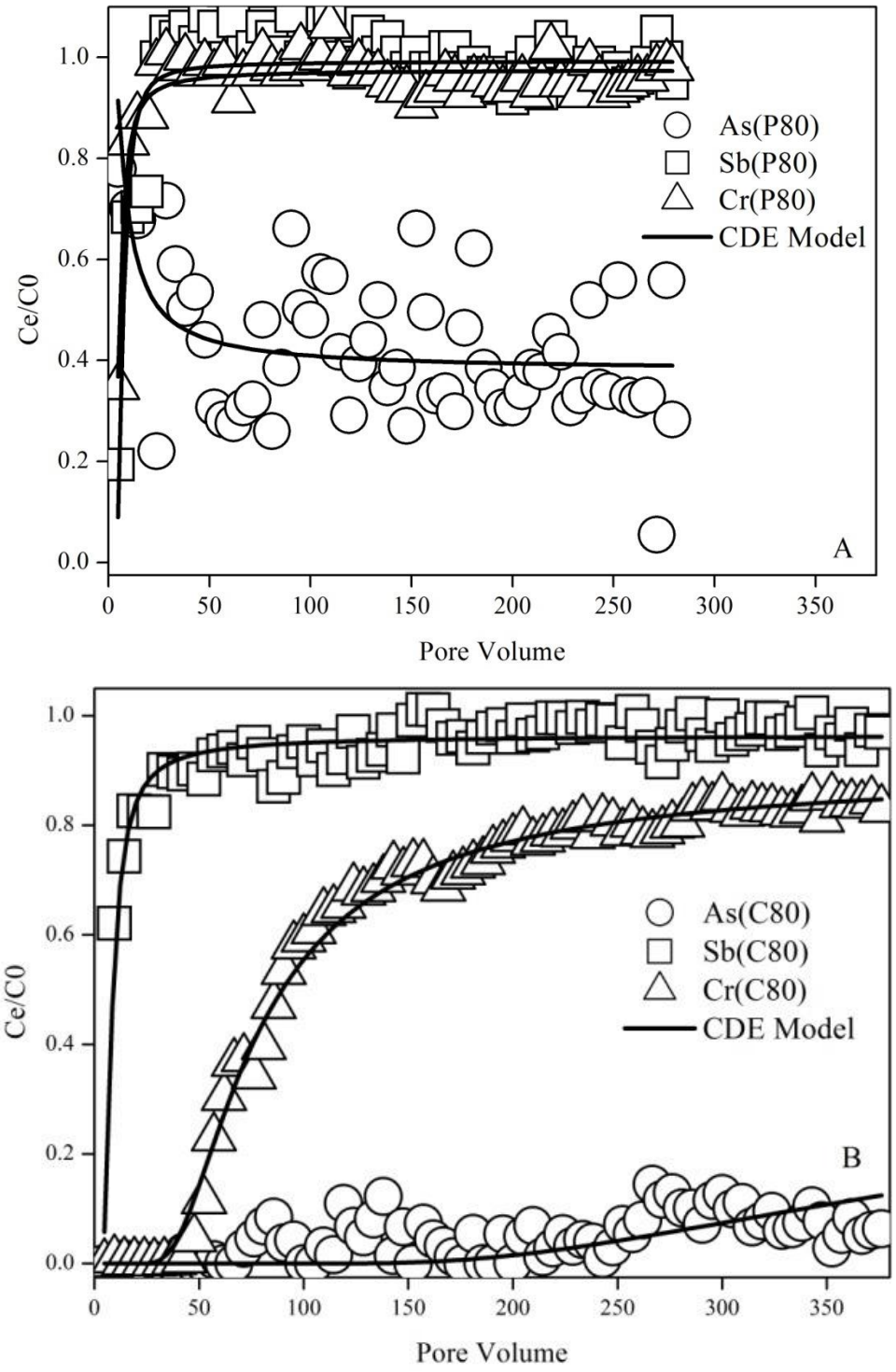
Ce/C0
Pore Volume
As(P80)
Sb(P80)
Cr(P80)
CDE Model
A
As(C80)
Sb(C80)
Cr(C80)
CDE Model
B

Figure 6.

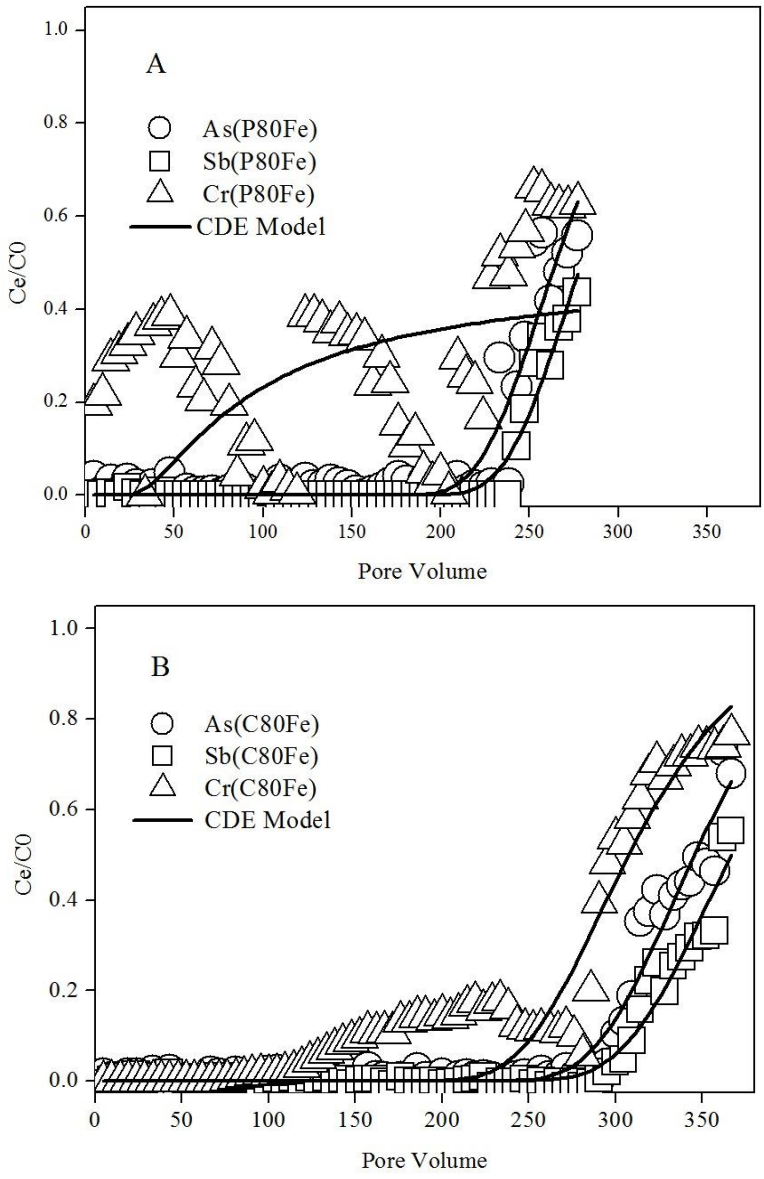
A
As(P80Fe)
Sb(P80Fe)
Cr(P80Fe)
CDE Model
Ce/C0
Pore Volume
B
As(C80Fe)
Sb(C80Fe)
Cr(C80Fe)
CDE Model
Ce/C0
Pore Volume

Figure 7.

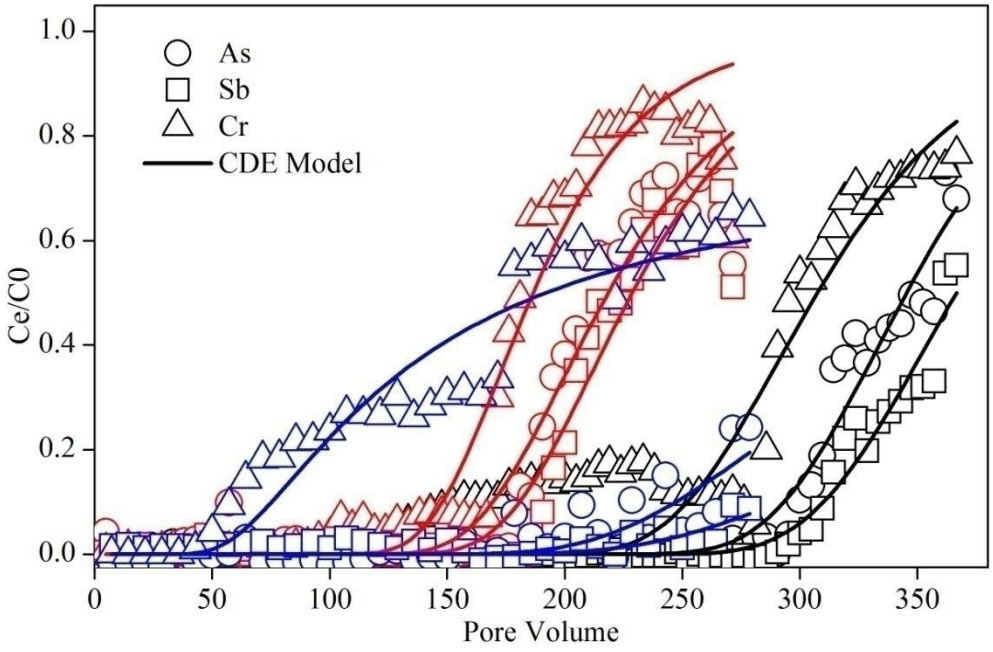

Flow rate (mL/h)	80 (black)	110 (red)	150 (blue)
Rf(As)	345	219	376
Rf(Sb)	367	228	492
Rf(Cr)	308	187	192

Figure 8.

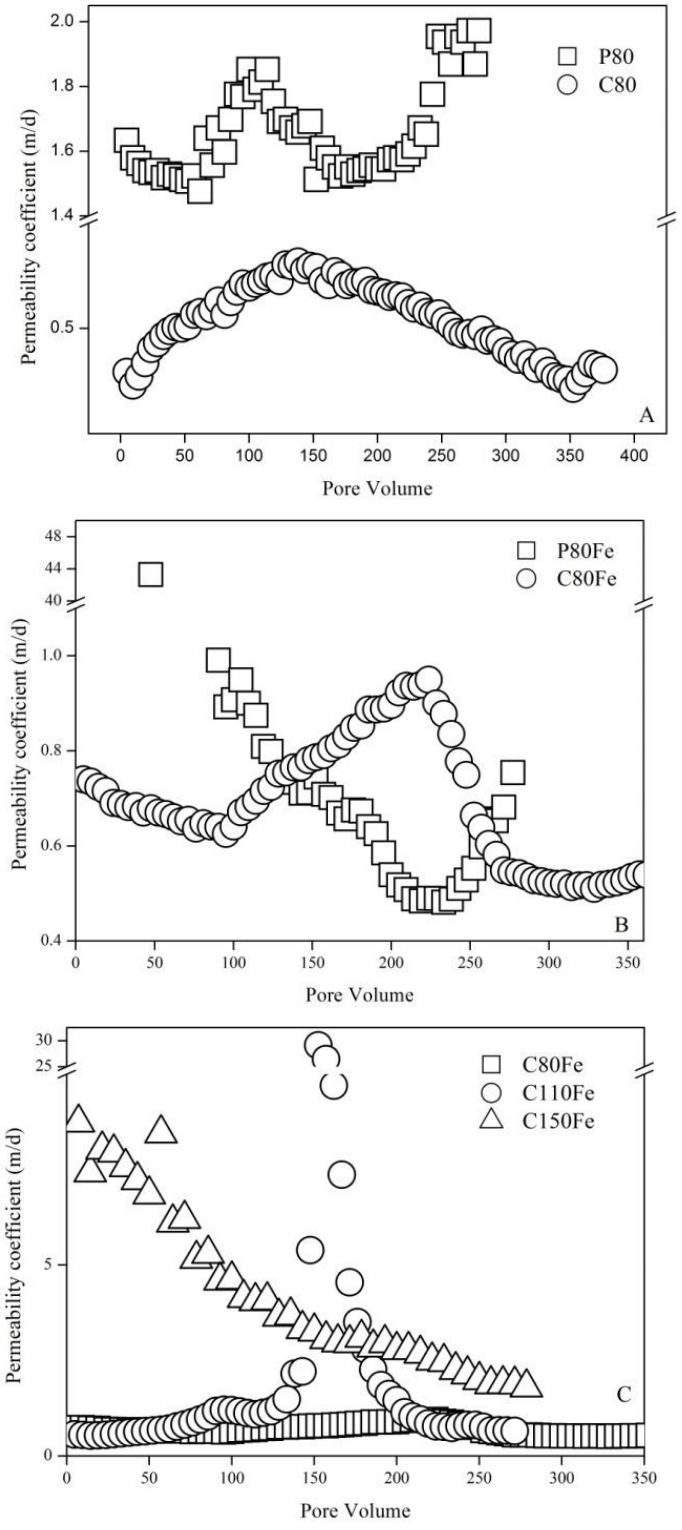
P80
C80
Permeability coefficient (m/d)
Pore Volume
A
P80Fe
C80Fe
B
C80Fe
C110Fe
C150Fe
C

Figure 9.

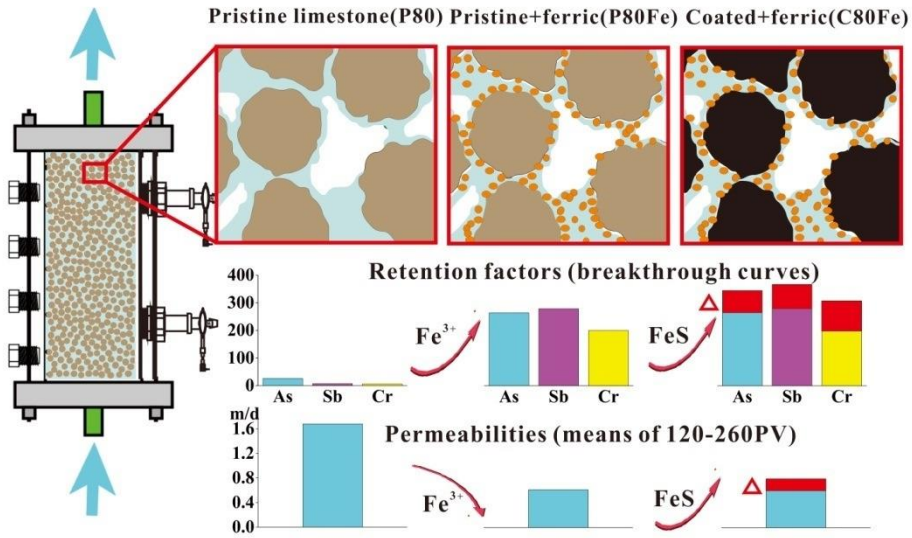

Figure 10.

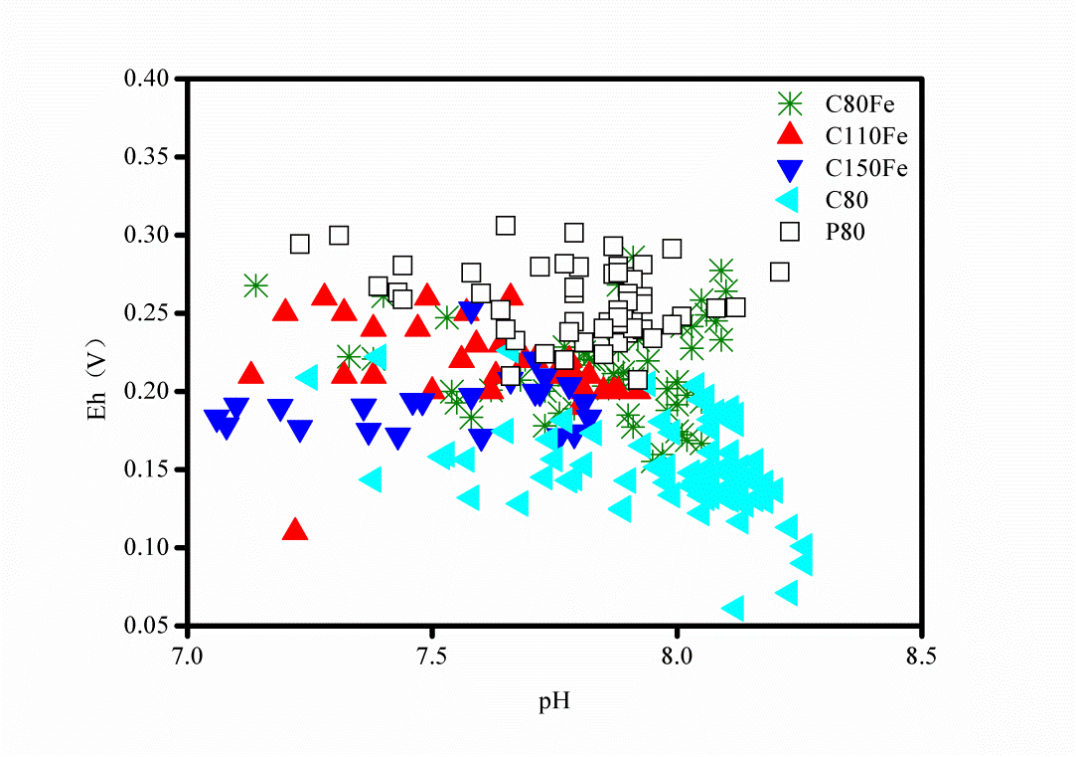

Supporting Information

Coupling effect of $Fe^{3+}_{(aq)}$ and biological, nano-sized FeS-coated limestone on the removal of redox-sensitive contaminants (As, Sb and Cr): implications for *in situ* passive treatment of acid mine drainage

Lei Zhou[1], Faqin Dong[1], Jing Liu[1], Karen A. Hudson-Edwards[2*]

[1]The Key Laboratory of Solid Waste Treatment and Resource Recycle, Ministry of Education, Southwest University of Science and Technology, Mianyang, 621010 China.

[2]Department of Earth and Planetary Sciences, Birkbeck, University of London, Malet St., London WC1E 7HX, UK.

*** Corresponding author: Karen A. Hudson-Edwards**

Phone: +44-(0)203 073 8030

E-mail: k.hudson-edwards@bbk.ac.uk

1. The basis for culturing and coating time of *A. cryptum* JF-5 and SRB

Optical density (OD) determined by spectrophotometer set at a wavelength of 595 nm can represent the amount of bacteria (Sánchez et al., 2005). For the SRB and JF-5 bacteria, the variation in concentration of SO_4^{2-} and Fe^{2+} can directly reflect the reduction performance according to the following reactions:

$$SO_4^{2-} + \text{Lactate} \xrightarrow{\text{SRB}} S^{2-} \quad (1)$$

$$Fe^{3+} + \text{Glucose} \xrightarrow{\text{JF-5}} Fe^{2+} \quad (2)$$

The quantity of bacteria and the reduction performance form the basis for determining the timings of column experiment. In order to determine the growth status and the main compositional concentrations of the media containing *A. cryptum* JF-5 and SRB, we recorded the growth curves of both microorganisms and concentrations of $Fe^{2+}_{(aq)}$ and $SO_4^{2-}{}_{(aq)}$. The aim is to ensure that limestones are coated by *A. cryptum* JF-5 and SRB at their highest concentrations of these ions.

As shown in Fig. S1, *A. cryptum* JF-5 is in a logarithmic growth phase when cultured in 3 days; this is the most rapid phase of bacterial growth. The growth of *A. cryptum* JF-5 reaches steady-state after culturing for 6 days. The growth of SRB is similar to that of JF-5. Therefore, *A. cryptum* JF-5 and SRB were pre-incubated inside an anaerobic chamber 6 days in advance of the actual experiments and the column containing the two bacteria was aged for and additional 72 h.

Concentrations of $Fe^{2+}_{(aq)}$ were measured using o-phenanthroline method. Concentrations of sulfate were measured by ion chromatography. The amount of bacteria was monitored by spectrophotometer at a wavelength of 595 nm.

2 .XRD of biological nano-sized FeS and batch adsorption schematic diagram

XRD analysis shows that the main mineral in the biological nano-sized FeS is mackinawite. The spectra also suggest that goethite and an unknown diffraction peak are present.

The batch adsorption experiment procedure is shown in Fig. S3. The maximum adsorption of As(V), Sb(V) and Cr(VI) on pristine limestone is 14.9, 9.9 and 9.2 μg/g, respectively, compared to 517, 596 and 1162 μg/g for the FeS-coated limestone. The results suggest that the nano-sized FeS particles coating the limestone improve the adsorption ability to a significant extent.

3. Color change of FeS-coated limestone column

Due to their rapid oxidation and difficulty in sampling, we did not collect samples from column for chemical analysis. The colour of the FeS-coated limestone column gradually changes from black to gray-green, eventually becoming brown-yellow (Fig. S4). This strongly suggests that redox reaction

has occurred between the FeS and the $Fe^{3+}_{(aq)}$, which affects the formation of ferric hydroxides.

4. Calibration of pressure sensors

To calibrate the pressure sensors, a pressure gauge connected with an injection syringe was used (Fig. S6). Different pressures values were obtained using a syringe injection to obtain a series of pressure values for the sensor and pressure values for the gauge. This permits determination of the intercept and slope which are important parameters of the pressure sensor program to calibrate the pressure sensor.

5. Statistical analysis of pH and Eh data

As shown in Fig. S7, all the pH and Eh values of the experiments lie along a straight line, showing that the data follow a normal distribution. Therefore, a Bartlett variance test can be performed to determine whether there are significant differences. The results are shown in Table S1, and they indicate that the FeS coating, $Fe^{3+}_{(aq)}$ and flow rate all contribute to the pH and Eh data having significant differences, because the p values are less than 0.05.

6. XPS As 3d peak spectra of Na_2HAsO_4

To achieve better contrast for the XPS spectra of the As-sorbed FeS samples and to illustrate the changes in the As 3d peak spectra, the XPS As 3d peak spectra of Na_2HAsO_4 was determined (Fig. S8).

6. Initial, during operation, and final physicochemical quality of effluents

The pH, Eh and electrical conductivity of effluents are presented in Figure S9, to help to understand the treatment process.

References

Rojas, F.S., Pavón, J.M.C., 2005. Spectrophotometry Biochemical Applications. Encyclopedia of Analytical Science (Second Edition), pp. 366-372.

Sánchez, B., Champomier-Vergès, M.-C., Anglade, P., Baraige, F., de los Reyes-Gavilán, C.G., Margolles, A., Zagorec, M., 2005. Proteomic analysis of global changes in protein expression during bile salt exposure of *Bifidobacterium longum* NCIMB 8809. J. Bacteriol. 187, 5799-5808.

Table S1. Bartlett hypothesis test results.

Estimation of least squares means	Test items			Comparison	P value
	P80	C80			
pH	7.807	7.979		P80<C80	0.000
Eh	0.2575	0.1514		P80>C80	0.000
Estimation of least squares means	Test items			Comparison	P value
	C80	C80Fe			
pH	7.979	7.840		C80>C80Fe	0.000
Eh	0.1514	0.2105		C80<C80Fe	0.000
Estimation of least squares means	Test items			Comparison	P value
	C80Fe	C110Fe	C150Fe		
pH	7.840	7.608	7.533	C80>C110>C150	0.000
Eh	0.2105	0.2176	0.1917	C80≈C110>C150	0.012

FIGURE CAPTIONS

Figure S1.

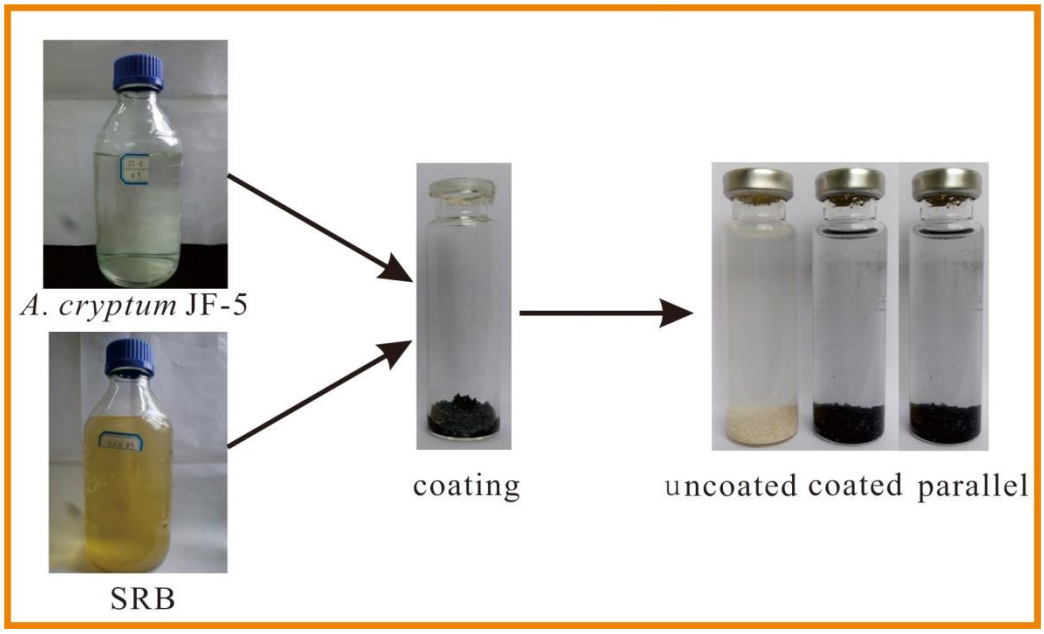

Figure S2.

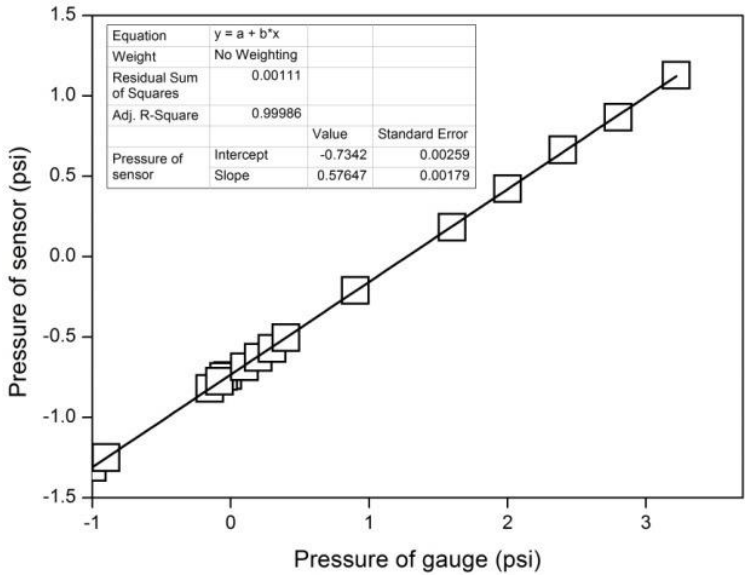

Figure S3.

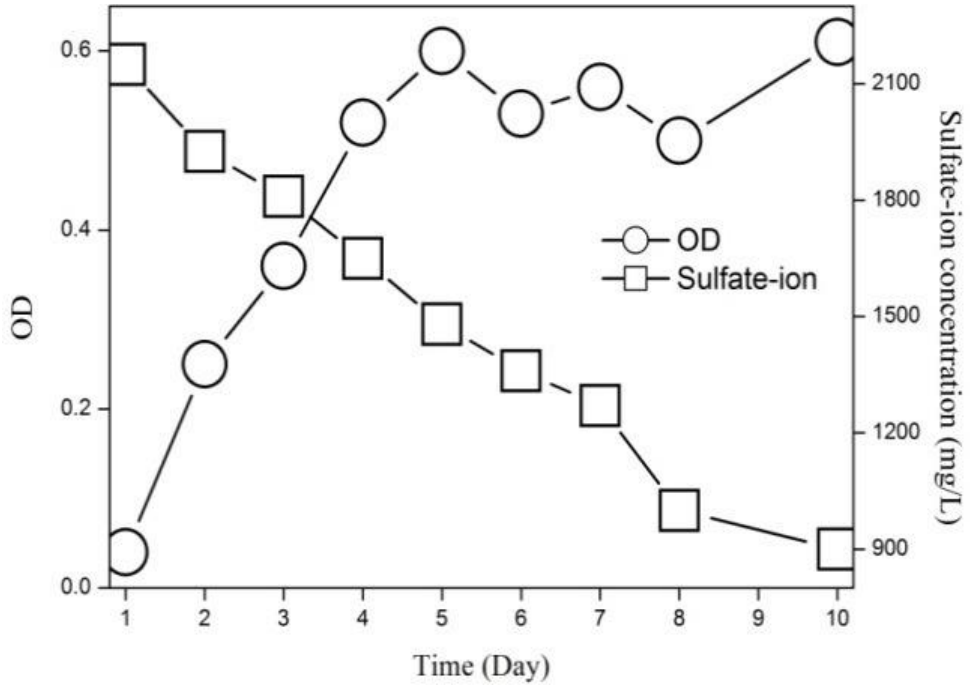

Figure S4.

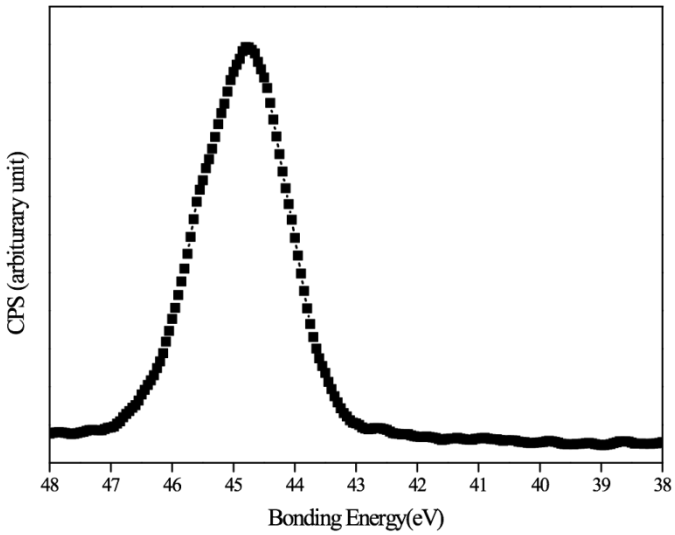

Figure S5.

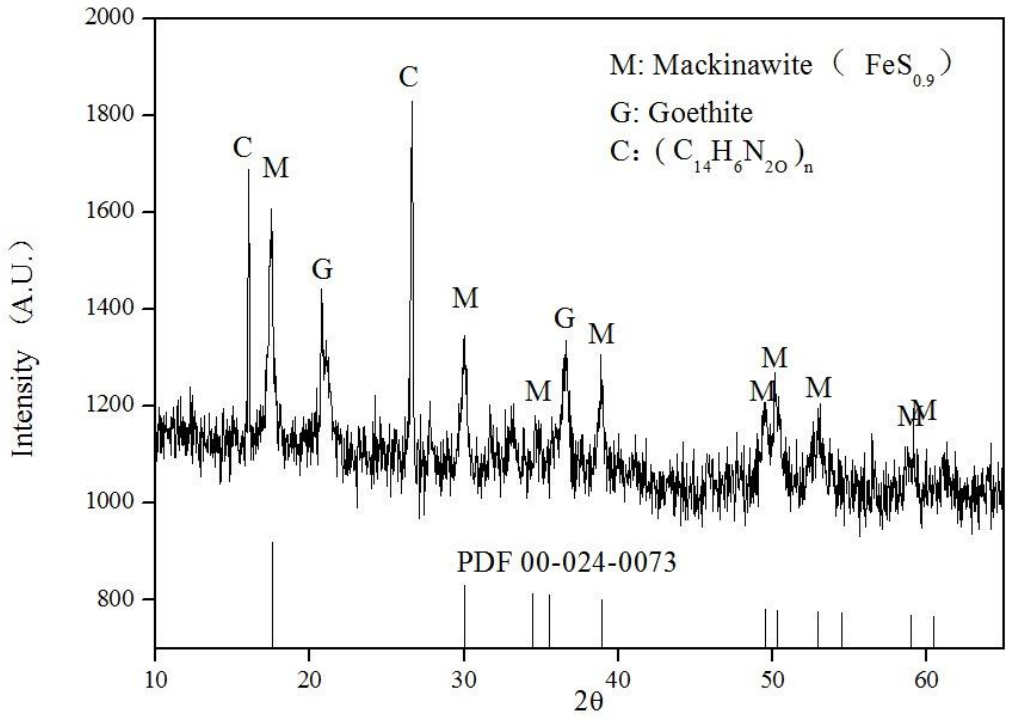

Figure S6.

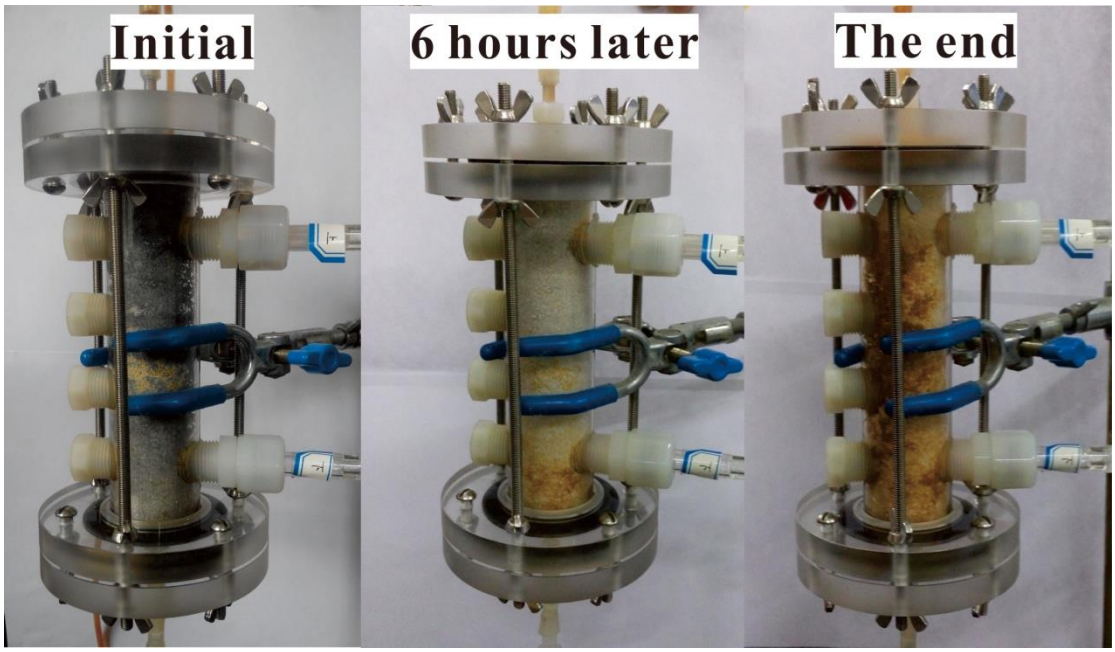

Figure S7.

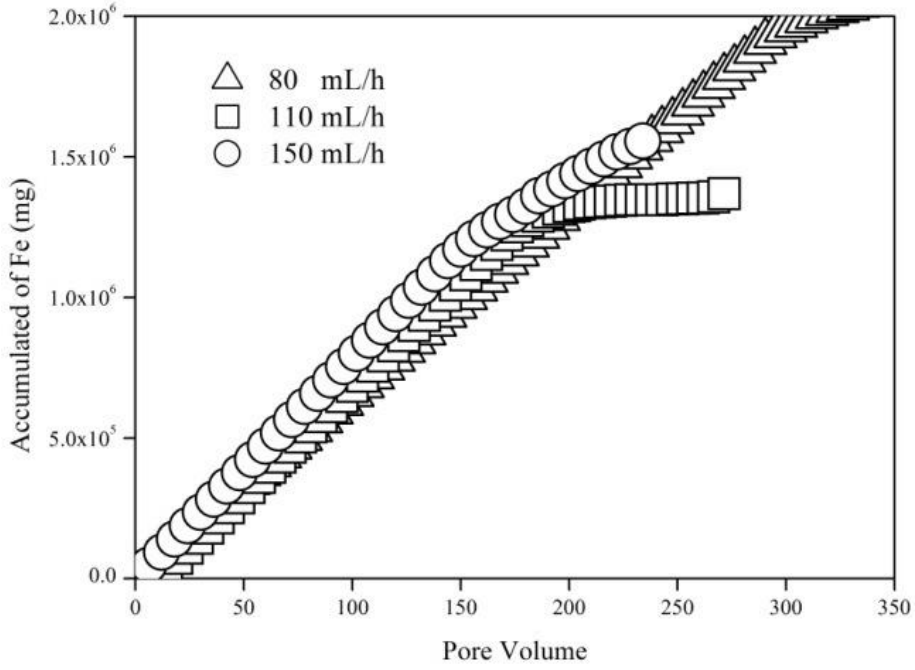
2.0x10^6
1.5x10^6
1.0x10^6
5.0x10^5
0.0
Accumulated of Fe (mg)
80 mL/h
110 mL/h
150 mL/h
0
50
100
150
200
250
300
350
Pore Volume

Figure S8.

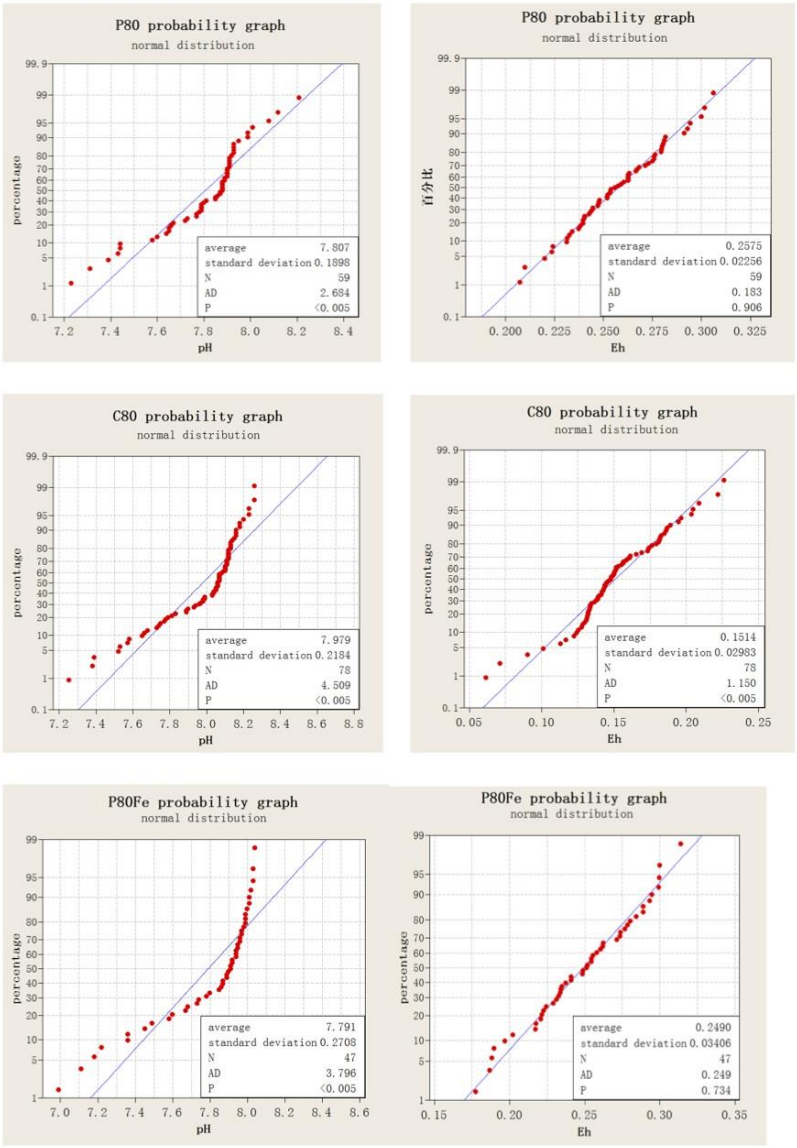
P80 probability graph
normal distribution
percentage
pH
average 7.807
standard deviation 0.1898
N 59
AD 2.684
P <0.005
P80 probability graph
normal distribution
百分比
Eh
average 0.2575
standard deviation 0.02256
N 59
AD 0.183
P 0.906
C80 probability graph
normal distribution
percentage
pH
average 7.979
standard deviation 0.2184
N 78
AD 4.509
P <0.005
C80 probability graph
normal distribution
percentage
Eh
average 0.1514
standard deviation 0.02983
N 78
AD 1.150
P <0.005
P80Fe probability graph
normal distribution
percentage
pH
average 7.791
standard deviation 0.2708
N 47
AD 3.796
P <0.005
P80Fe probability graph
normal distribution
percentage
Eh
average 0.2490
standard deviation 0.03406
N 47
AD 0.249
P 0.734

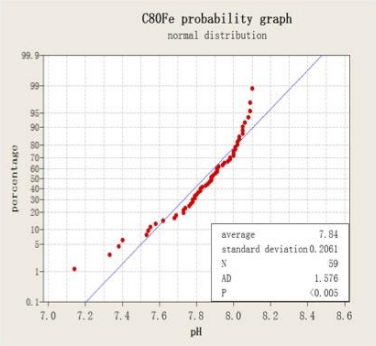
C80Fe probability graph
normal distribution
percentage
pH
average 7.84
standard deviation 0.2061
N 59
AD 1.576
P <0.005

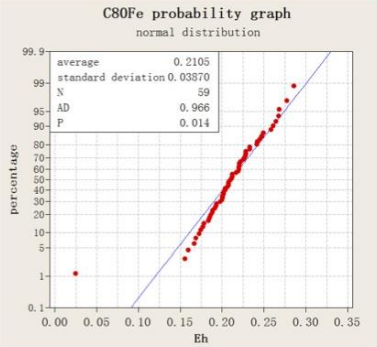
C80Fe probability graph
normal distribution
percentage
Eh
average 0.2105
standard deviation 0.03870
N 59
AD 0.966
P 0.014

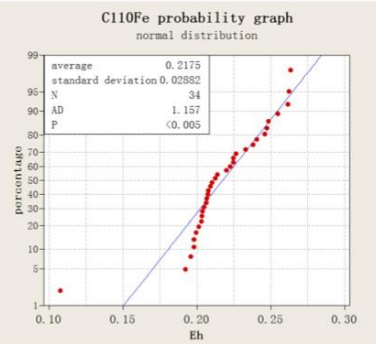
C110Fe probability graph
normal distribution
percentage
Eh
average 0.2175
standard deviation 0.02882
N 34
AD 1.157
P <0.005

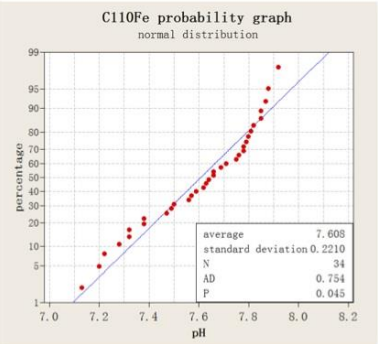
C110Fe probability graph
normal distribution
percentage
pH
average 7.608
standard deviation 0.2210
N 34
AD 0.754
P 0.045

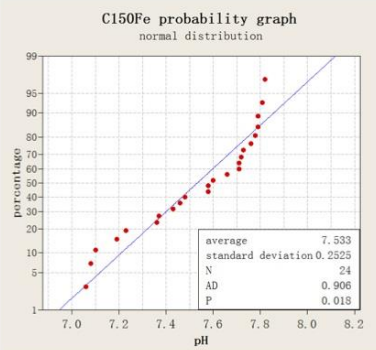
C150Fe probability graph
normal distribution
percentage
pH
average 7.533
standard deviation 0.2525
N 24
AD 0.906
P 0.018

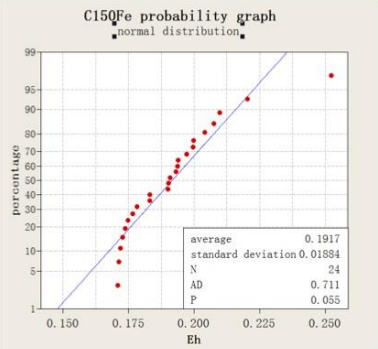
C150Fe probability graph
normal distribution
percentage
Eh
average 0.1917
standard deviation 0.01884
N 24
AD 0.711
P 0.055

Figure S9.

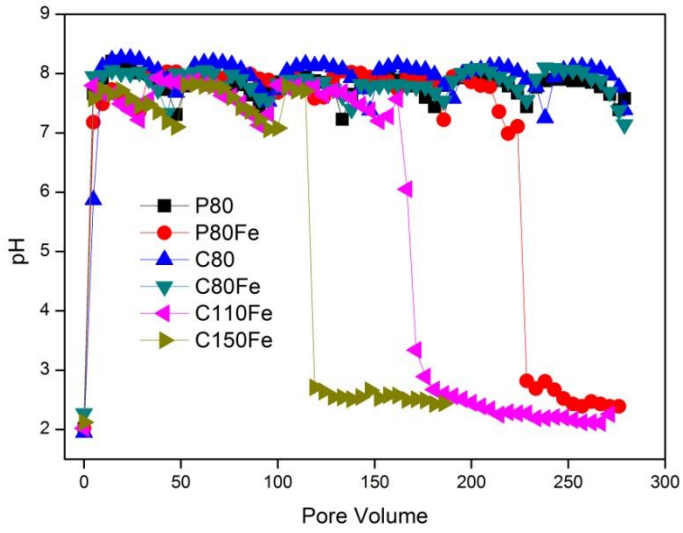
pH
Pore Volume
P80
P80Fe
C80
C80Fe
C110Fe
C150Fe

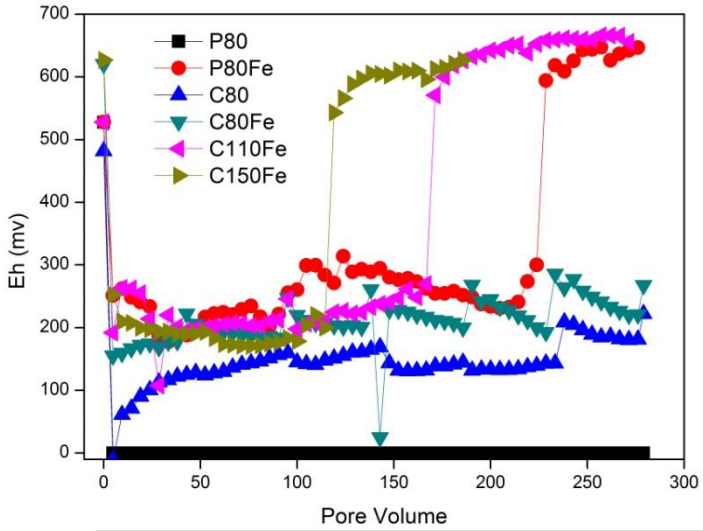
Eh (mv)
Pore Volume
P80
P80Fe
C80
C80Fe
C110Fe
C150Fe

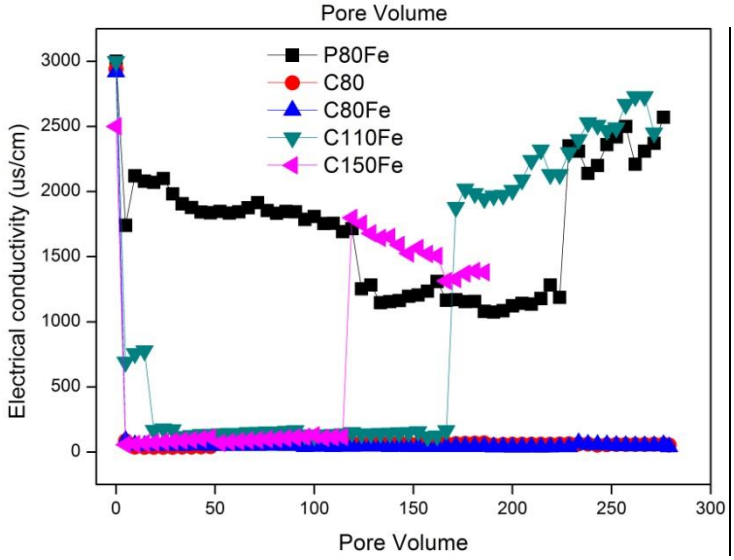
Electrical conductivity (us/cm)
Pore Volume
P80Fe
C80
C80Fe
C110Fe
C150Fe